Published in final edited form as:

Glia. 2021 June ; 69(6): 1563–1582. doi:10.1002/glia.23979.

TRPV4 channels mediate the mechanoresponse in retinal microglia

Sarah N. Redmon[1], **Oleg Yarishkin**[1], **Monika Lakk**[1], **Andrew Jo**[1], **Edin Mustafic**[1], **Peter Tvrdik**[5], **David Križaj**[1,2,3,4]

[1]Department of Ophthalmology & Visual Sciences, Moran Eye Institute, Salt Lake City, UT 84132

[2]Interdepartmental Program in Neuroscience, University of Utah, Salt Lake City, UT 84132

[3]Department of Bioengineering, University of Utah, Salt Lake City, UT 84132

[4]Department of Neurobiology & Anatomy, University of Utah, Salt Lake City, UT 84132

[5]Department of Neurological Surgery, University of Virginia School of Medicine, Charlottesville VA 22908

Abstract

The physiological and neurological correlates of plummeting brain osmolality during edema, traumatic CNS injury and severe ischemia are compounded by neuroinflammation. Using multiple approaches, we investigated how retinal microglia respond to challenges mediated by increases in strain, osmotic gradients and agonists of the stretch-activated cation channel TRPV4. Dissociated and intact microglia were TRPV4-immunoreactive and responded to the selective agonist GSK1016790A and substrate stretch with altered motility and elevations in intracellular calcium ($[Ca^{2+}]_i$). Agonist- and hypotonicity-induced swelling was associated with a nonselective outwardly rectifying cation current, increased $[Ca^{2+}]_i$ and retraction of higher-order processes. The antagonist HC067047 reduced the extent of hypotonicity-induced microglial swelling, and inhibited the suppressive effects of GSK1016790A and hypotonicity on microglial branching. Microglial TRPV4 signaling required intermediary activation of phospholipase A2 (PLA2), cytochrome P450, and production of epoxyeicosatrienoic acids (EETs). The expression pattern of vanilloid *thermoTrp* genes in retinal microglia was markedly different from retinal neurons, astrocytes and their cortical counterparts. These results suggest that TRPV4 represents a primary retinal microglial sensor of osmochallenges under physiological and pathological conditions. Its activation, associated with PLA2, modulates calcium signaling and cell architecture. Antagonizing TRPV4 channels might be a useful strategy to suppress microglial overactivation in the swollen and edematous CNS.

Graphical Abstract

CORRESPONDING AUTHOR: David Križaj, 65 N Mario Capecchi Drive, Bldg. 523, Room S4140 JMEC, Salt Lake City, UT 84132. david.krizaj@hsc.utah.edu.

COI STATEMENT: The authors declare that no conflict of interest exists.

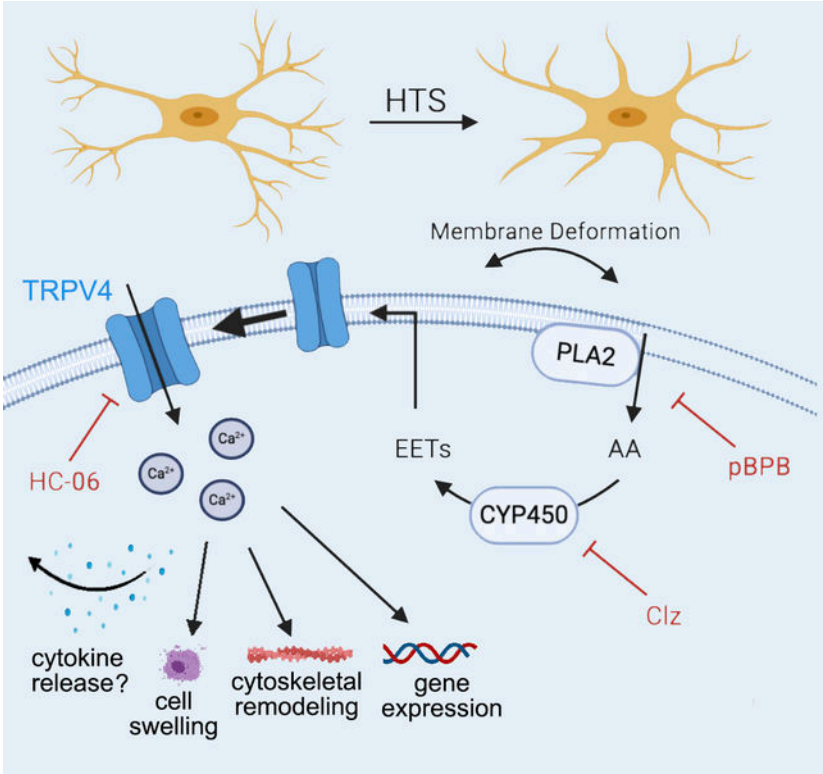

Keywords

retina; microglia; TRPV4; osmotransduction; volume regulation; edema

Introduction

Changes in osmotic gradients trigger an immediate redistribution of water between intra- and extracellular CNS compartments (Krizaj et al., 1996; Murphy et al., 2017) with attendant and potentially disruptive changes in neuronal excitability and cognitive function (Renneboog et al., 2006; Risher et al., 2009; Wittbrodt et al., 2018). Swelling of CNS glia and immune cells occurs during hypoxia, ischemia, hyponatremia, hypothermia and diabetic ketoacidosis (Hoffmann et al., 2009; Kimelberg, 2005) and was observed in upwards of 25% of patients hospitalized after traumatic brain injury, acute liver failure, stroke and neurosurgery (Donkin & Vink, 2010). In the retina, edema associated with glial swelling, dysregulation of transglial water transport and microglial accumulation may interfere with photon transmission and damage cell layers in metabolic, vascular and inflammatory diseases, thereby contributing to vision loss (Gardner et al., 2002; Bringmann et al., 2004; Pannicke et al., 2006; Holborn et al., 2008; Otani et al., 2009; Sun et al., 2015; Daruich et al., 2018).

Microglia are ramified and structurally dynamic immune cells that maintain CNS homeostasis through secretion of neurotrophic factors, removal of damaged cells and synapses, and vascular remodeling (Arcuri et al., 2017; Salter & Stevens, 2017),

with brain regions showing notable differences in the density, turnover, metabolism, electrophysiological properties and transcriptional patterns of resident microglia (DeBiase et al., 2017; Silvin and Ginhoux, 2018). In the healthy adult retina, microglia are ramified and surveil the local environment in the two synaptic layers to clear metabolic products, phagocytose cell debris, and modulate intercellular communication. Focal injury, aging and chronic degeneration (retinitis pigmentosa, diabetic retinopathy, glaucoma) promote microglial proliferation, adoption of amoeboid morphology, transition towards migratory phenotypes, and cytokine secretion (Tang et al., 2011; Yu et al., 2020; O'Koren et al., 2019) during the initiation and perpetuation stages of the degenerative process. The 'activated' state has been associated with increased $[Ca^{2+}]_i$ and release of reactive radicals and cytokines (Hoffmann et al., 2003; Tvrdik & Kalani, 2017). While human and rodent microglia can be activated by cerebral edema and rapid corrections of osmotic imbalances (Jiang et al., 2009; Zemtsova et al., 2011) to mediate the neuroinflammatory response (Gankam-Kengne et al., 2010; Gong et al., 2004; Starkey et al., 2017; Tanaka et al., 2018), there is surprisingly little information about whether microglia are capable of *in situ* osmosensing of physiological and pathological osmogradients, how osmotic gradients influence microglial signaling and what the swelling sensors might be.

A candidate mechanism by which microglia could sense local osmolality decreases is TRPV4 (transient receptor potential vanilloid isoform 4), a nonselective cation channel that is activated by cell swelling, stretch and shear flow (Diaz-Otero et al., 2018; Mola et al., 2016; Ryskamp et al., 2014a; Toft-Bertelsen et al., 2017). TRPV4 was suggested to suppress cortical microglial activation (Konno et al., 2012), however, in retinal macroglia the channel promotes cytokine release and reactive gliosis (Krizaj et al., 2014; Taylor et al., 2017; Matsumoto et al., 2018), together with proinflammatory functions in nociception and mechanical hyperalgesia across the CNS (Alessandri-Haber et al., 2003; Henry et al., 2016; Redmon et al., 2017). It is currently not known how microglial TRPV4 channel is activated by mechanical stressors, nor how ramified cells in the intact CNS respond to physiological and pathological osmotic gradients. Here, we take advantage of the *ex vivo* retinal preparation which has no discernible effects on microglial activation (Fontainhas et al., 2011) to identify TRPV4 as a principal transducer of osmotic and mechanical stress. In the current study we demonstrate that TRPV4 mediates the microglial response to swelling and stretch, determine that this process requires production of eicosanoid messengers and show that TRPV4-mediated Ca^{2+} influx is associated with dramatic changes in microglial architecture and motility. The quasi-reactive, less-ramified, phenotype induced by TRPV4 agonists and osmotic stressors suggests that the biomechanical milieu directly modulates retinal microglial signaling. Furthermore, the efficacy of TRPV4 antagonists in preserving microglial architecture in the presence of severe hypotonic stress suggests that targeting the channel might help alleviate neuroinflammatory activation in the edematous CNS.

Materials and Methods

Animals.

Adult C57BL/6J (RRID:IMSR_JAX:000664), $CX3CR1^{GFP/+}$ (RRID: MGI:2670353), bacterial artificial chromosome (BAC)-transgenic Tg(TRPV4-EGFP)MT43Gsat mice

(TRPV4^{eGFP}; RRID:MMRC_032771-UCD; Gu et al., 2016), and *Aif1*(Iba1)-IRES-Cre; PC::GCaMP5-tdT mice (Gee et al., 2014; Pozner et al., 2015) between 2–6 months of age were maintained in a pathogen-free facility with a 12-hour light/dark cycle and unrestrained access to food and water. Data from male and female mice were pooled as no gender differences were noted. The genotype of CX3CR1$^{GFP/+}$ mice was confirmed by PCR from tail snips using the primers: WT-F (5'-GTC TTC ACG TTC GGT CTG GT-3'), CMMN-R (5'-CCC AGA CAC TCG TTG TCC TT-3') and MUT-F (5'-CTC CCC CTG AAC CTG AAA C-3'). PCR was performed using the following protocol: 94°C for 2 min; 10 cycles of 94°C for 20 sec, 60°C for 30 sec (decreasing 0.5°C per cycle), 68°C for 30 sec; 28 cycles of 94°C for 20 sec, 55°C for 30 sec, 72°C for 30 sec; 72°C for 2 min and then held at 4°C until run on a 2% agarose gel. The protocols adhered to the NIH Guide for the Care and Use of Laboratory Animals and were approved by the Institutional Animal Care and Use Committees at the University of Utah. It is worth noting that the process motility and physiology of CX3CR1$^{GFP/+}$ microglia are indistinguishable from wild type cells (Ré et al., 2006; Wake et al., 2009).

Reagents.

Salts and reagents were purchased from MilliporeSigma except where noted otherwise. The TRPV4 agonist GSK1016790A and antagonist HC-067047 (HC-06) were purchased from MilliporeSigma (Cat. Nos.: 530533, 616521). Arachidonic acid (AA, Cat. No. 90010), its metabolites (5',6'-EET: Cat. No.:50211, 11',12'-EET: Cat. No. 50511) and enzymatic antagonists clotrimazole (Ctz) (Cat. No.: 15278) and p-bromophenacylbromide (pBPB) (Cat. No.: D38308) were obtained from Cayman Chemical. Due to AA autohydrolyzation, the lipids were aliquoted, gassed with liquid nitrogen and stored at −80°C until use. Adenosine 5'-triphosphate magnesium salt was obtained from MilliporeSigma (Cat. No.: A9187). Saline, adapted from Lee et al. (2008), contained (in mM): NaCl 60, KCl 5, NaH_2PO_4 1.25, $MgCl_2$ (6H20) 0.75, $CaCl_2$ 1.5, glucose 10, HEPES 20. pH was set at 7.4 and osmolarity set to 300 mOsm. Extracellular osmolarity was set by addition or removal of mannitol, a procedure that minimally disrupts ionic strength of the extracellular solution. Osmolarity was checked thermometrically using a vapor pressure osmometer (Wescor, Logan, UT).

Acutely Dissociated Microglia Preparation.

CX3CR1$^{GFP/+}$ mice were euthanized, enucleated and retinas isolated in cold Leibovitz 15 (L15) medium (ThermoFisher Scientific, Cat. No. 41300039) containing 11 mg/ml L15 powder, 20 mM D-glucose, 10 mM Na-HEPES, 2 mM sodium pyruvate, 0.3 mM sodium ascorbate, and 1 mM glutathione. To digest the extracellular matrix, retinas were incubated in L-15 containing papain (7 U/ml; Worthington, Cat. No.: LS003119) for 1 hour at RT. Retinas were rinsed, placed on ice and cut into 500 μm pieces. 1–2 of these pieces were triturated and plated on concanavalin A (0.4 mg/ml; Alfa Aesar, Cat. No.: J61221)-coated coverslips. Dissociated cells were loaded with Fura-2 AM or Fura-5F AM (5–10 μM; Invitrogen/ThermoFisher, Cat. Nos. F1221 & F14177, respectively) for 30–40 min and washed for 10–20 min. Under our experimental conditions, most plated cells maintained low baseline $[Ca^{2+}]_i$ at 22°C for several hours without substantial shifts in the baseline, as observed for other ocular cells (Jo et al., 2016; Molnar et al., 2012; Ryskamp et al., 2011,

2016; Szikra et al., 2009;). Microglia were identified by GFP-reporter fluorescence, and identity was confirmed by post-imaging immunocytochemistry.

Magnetic-activated cell sorting (MACS).

The sorting protocol was modified from Lakk et al. (2018), as follows. Mouse retina and cortex was dissociated with 16 U/ml papain (Worthington, 50 U/ml DNase I (Roche/ThermoFisher, Cat. No. 4716728001) and 10 mM glucose for 1 hour at 37 °C, followed by trituration in PBS 1.5 mg/ml BSA, 1.5 mg/ml Trypsin inhibitor at pH 7.4, yielding a single cell suspension that was passed through a 70 μm pre-separation filter (Miltenyi Biotech, Cat. No.: 130-095-823) and centrifuged. To purify microglia, Müller cells or RGCS, the pellet was re-suspended and incubated in 0.5 % BSA solution containing CD11b, anti-biotin, CD90.1-coated microbeads, respectively (1:10; Miltenyi Biotech, Cat. No. 130-093-634, 130-090-485, 130-121-273, respectively) for 15 min at 4°C. To isolate Müller cells, the pellet was incubated with biotinylated hamster anti-CD29 (clone Ha2/5, BD Biosciences, Cat. No. 555004) for 15 min at 4°C. After additional washing and centrifugation, cells were washed through MACS filter columns and the cells were eluted in DMEM medium (Gibco/ThermoFisher Scientific, Cat. No. 11885–084) with 1% penicillin/streptomycin (pen/strep; Sciencell, Cat. No.: 0513), 10% FBS (Lonza, Cat. No.: CC-4102FF). RGCs were eluted in serum-free Neurobasal medium (Gibco/ThermoFisher, Cat. No.: 21103–049) with 1% penicillin/streptomycin (Sciencell), transferrin (0.1 mg/ml; MilliporeSigma, Cat. No.: T8158), putrescine (16 ng/ml; Sigma, Cat. No.: P5780), insulin (5 ng/ml; MilliporeSigma, Cat. No.: I6634), 3,5,3-trioodothyronine T3 (100 nM; MilliporeSigma, Cat. No.: T2877), progesterone (20 nM; ACROS Organics, Cat. No.: AC225650050), 2% B27 (Thermo Fisher, Cat. No.: 17504044), N-acetyl cysteine (5 ng/ml; MilliporeSigma, Cat. No.: A9165), sodium pyruvate (1 mM; MilliporeSigma, Cat. No. P5280), L-glutamine (2 mM; Invitrogen, Cat. No.: 25030149), brain-derived neurotrophic factor (BDNF, 50 ng/ml; GenWay Biotech, Cat. No.: GWB-7ED615), ciliary neurotrophic factor (CNTF, 10 ng/ml; GenWay Biotech, Cat. No.: GWB-56D467) and forskolin (5 μM; Thermo Fisher, Cat. No.: BP25201). The growth medium was changed every 2–3 days. Quantification of cells negative for Iba1 (i.e., photoreceptors, RGC, Müller cells, etc.) showed 11.3 ± 2.2% contamination.

Reverse Transcription and Polymerase Chain Reaction (PCR).

Total RNA was isolated using Arcturus PicoPure RNA Isolation Kit according to the manufacturer instructions (ThermoFisher, Cat. No.: KIT0204). 100 nanogram of total RNA was used for reverse transcription. First-strand cDNA synthesis and PCR amplification of cDNA were performed using qScript™ XLT cDNA Supermix (Quanta Biosciences, Cat. No.:95161). To visualize PCR products, samples were run on 2% agarose gels using ethidium bromide staining, along with 100-bp DNA ladder (ThermoFisher Scientific, Cat. No.: S0323). The PCR products are displayed in Figure 1D.

Quantitative Real-Time Polymerase Chain Reaction (qRT-PCR).

Sybergreen based real-time PCR was performed using Apex qPCR GREEN Master Mix (Genesee Scientific, Cat. No.: 42-119PG). The results were performed in triplicate for at least four separate experiments. The comparative C_T method ($\Delta\Delta C_T$) was used to measure and quantify relative gene expression where the fold enrichment was calculated as $2 - [\Delta C_T$

(sample) – ΔC_T(calibrator)] after normalization. To normalize fluorescence signals, GAPDH and β-actin were utilized as endogenous controls. The primer sequences are given in Table 1.

Immunohistochemistry.

The immunolabeling protocol for vertical sections followed the procedures described in Molnár et al. (2016) and Lakk et al. (2018). Eyes from adult mice were removed after euthanasia, punctured with a needle at the ora serrata and placed in 4% paraformaldehyde in phosphate buffered saline (PBS) for 1 hour. Eyecups were sequentially dehydrated in 15 and 30% sucrose and embedded in OCT mounting medium. 12–14 μm thick cryosections were mounted onto Superfrost Plus slides. Before immunohistochemistry, excess OCT was removed, and sections were incubated in a blocking buffer (5% FBS and 0.3% Triton X-100 in 1X PBS) for 30 minutes. Dissociated cells were prepared as described and then fixed in 4% PFA in PBS for 10 minutes. Microglia were identified by GFP fluorescence. Whole-mounted retinas were prepared from isolated TRPV4e^{GFP} mice and immunostained for Iba1. Briefly, isolated retinas were fixed in 4% PFA for 30 min at RT, incubated in blocking buffer for 1 hour and incubated with a primary antibody, rabbit anti-Iba1 (ionized Ca^{2+}-binding adaptor molecule 1; 1:500; Fujifilm Wako PureChemical, Cat. No.: 019–19741) in antibody dilution buffer (2% BSA, 0.3% Triton-X in 1X PBS). Retinas prepared from CX3CR1$^{GFP/+}$ mice were prepared as described above, and incubated with rabbit anti-TRPV4 (1:1000; LifeSpan Biosciences, Cat. No.: LS-C110035) as the primary antibody. The tissue was incubated overnight (vertical sections and dissociated cells) or 3 days (whole-mounts) at 4°C, rinsed, and a secondary antibody (Alexa 594 goat anti-rabbit IgG; 1:1000, LifeSpan Biosciences, Cat. No. LS-C752285-100) applied for 1 hour at RT. After a final wash (3× 1X PBS for 5 min), the preparations were protected with Fluoromount-G + DAPI (Thermo Fisher Scientific, Cat. No. 010020), coverslipped and imaged on an Olympus FV1200 confocal microscope using 488 nm Ar (10%) and 543 nm He/Ne (10%) lasers for fluorophore excitation and 20x (1.0 N.A. water), 40x (0.8 N.A. water), and 40x (1.3 N.A. oil) objectives.

Cell Swelling Assays.

Volume regulation assays in retinal microglia were conducted as described (Jo et al., 2015, 2016) following the protocol originally devised by Chiavaroli et al. (1994). Fura-2 fluorescence emission after alternate excitation at 340 and 380 nm was normalized to baseline fluorescence and summed ($F_{vol} = F_{340} + F_{380}/x$, where x – 1–3, a value derived empirically for each experiment to calcium-dependent and opposing changes in F_{340} and F_{380}). This eliminated Ca^{2+}-dependence from traces and thus remaining changes in fluorescence reflected changes in intracellular volume. Cell volume is proportional to $\sqrt{area^3}$ when swelling occurs uniformly in all directions, which we confirmed with confocal z-stacks over time (data not shown). 3D volumes were analyzed in ImageJ.

Electrophysiology.

Retinal wholemounts were placed in the recording chamber and superfused with oxygenated saline. Microglia within the inner plexiform layer (IPL) were visualized by the expression of the eGFP reporter. Patch pipettes were pulled from borosilicate glass capillaries (WPI)

with a Sutter Instruments Puller (Novato, CA), with 10 – 12 MΩ resistance (Jo et al., 2015; Yarishkin et al., 2020). The extracellular solution contained (mM): 140 NaCl, 2.5 KCl, 1.5 $MgCl_2$, 2.0 $CaCl_2$, 5.5 D-glucose, 10 HEPES, (pH was adjusted with NaOH to 7.4). The pipette solution contained (mM): 125 Cs-$MeSO_4$, 10 HEPES, 2 $MgCl_2$, 2 Mg-ATP, 1 $CaCl_2$, 10 EGTA. The pipette solution used in the experiments with dissociated acutely dissociated microglia contained (mM): 125 K-gluconate, 10 KCl, 10 HEPES, 2 $MgCl_2$, 4 Mg-ATP, 10 EGTA. Whole-cell trans-membrane currents were recorded with a Multiclamp 700B amplifier and Digidata 1440A interface (Molecular Devices). Currents were acquired with pCLAMP 10.0, sampled at 10 kHz and filtered at 2 kHz. Currents were elicited by RAMP pulses ascending from −100 mM to 100 mV from the holding potential of −80 mV. RAMP pulses had 1-sec duration, and they were applied at a frequency of 0.2 Hz. All solutions were oxygenated with carbogen (95% O_2, 5% CO_2) for 30 minutes before setting the pH to 7.4 and experiments were performed at RT (22 – 23°C).

In vitro calcium imaging.

Ratiometric time-lapse Ca^{2+} imaging was conducted as described (Lakk et al., 2017; Ryskamp et al., 2014) using inverted or upright Nikon microscopes and 20x (0.75 N.A. oil) or 40x (1.3 N.A. oil; 0.8 N.A. water) objectives. Cells were loaded with the calcium-sensitive indicator Fura-2 AM (5–10 μM; stock solution in DMSO) for 40 min. The intracellular concentration of the de-esterified dye was assumed to be ~100 μM (Krizaj & Copenhagen, 1998). Excitation was provided via sequential exposure to 340 nm and 380 nm wavelengths that were delivered by Lambda DG-4 illumination systems (Sutter Instruments, Novato, CA). The images were captured with 14-bit CoolSNAP HQ^2 or Delta Evolve cameras (typically, binned at 2×2 or 4×4 pixels, at 0.5 Hz) and processed with NIS-Elements (Nikon/Technical Instruments). The data, collected as emission ratios for 340 nm and 380 nm excitations (F_{340}/F_{380}) are presented as ΔR/R. A subset of cells was calibrated as described previously (Krizaj et al., 1999; Szikra et al., 2009) with 10 μM ionomycin, 10 mM Ca^{2+} and 0 Ca^{2+}/3 mM EGTA. The apparent $[Ca^{2+}]_i$ was determined from the equation $[Ca^{2+}]_i = ((R - R_{min})/(R_{max} - R)) \times (F^{380}max/F^{380}min) \times K_d$, where R is the ratio of emission intensity at 510 nm evoked by 340 nm excitation versus emission intensity at 510 nm evoked by 380 nm excitation, R_{min} is the ratio at zero free Ca^{2+}, R_{max} is the ratio at saturating Ca^{2+}, and the dissociation constant K_d for Ca^{2+}-Fura 2 at room temperature was taken to be 224 nM (Krizaj and Copenhagen, 1998).

Two-photon imaging.

Unlike craniotomies and thinned-skull preparations (Marker et al., 2010), *ex vivo* adult retinal microglia maintain the resting process length, dendritic complexity and velocity (Faits et al., 2016; Fontainhas et al., 2011; Wang et al., 2014). Our studies in Iba1-Cre:GCaMP5 and $CX3CR1^{GFP/+}$ retinas were conducted in RGC side- up flat-mounts that were secured on a glass coverslip with a harp. Oxygenated (95% O_2/5% CO_2) saline was perfused at 5 ml/min via a peristaltic pump (Dynamax, USA). A W-Series was used to determine the optimal wavelength for GFP (870 nm) or simultaneous GCaMP5/tdT (920 nm) imaging. Imaging was conducted using the two-photon microscope (Ultima II; Bruker) with the Mai Tai laser (SpectraPhysics) tuned to 870 or 920 nm. To avoid photodamage, the maximal output of the laser power at the sample was kept low (< 20 mW). Signal

was acquired with GaAsP detectors using a 490–560 nm bandpass filter for GCaMP5G. For all GCaMP5 experiments image were collected from a single plane of view and images obtained every 1–3 seconds at 512 × 512 pixels. For all morphology experiments, a Z-stack was typically collected over 4–5 minutes. Z-stacks were set to include all microglial processes within the inner retina (RGC/NFL and IPL). Images were obtained with a 20x objective (1.0 N.A. water, Olympus) at 1024 × 1024 pixels. To account for changes in retinal thickness during hypotonic conditions (Hermoso et al., 2004; Ryskamp et al., 2014), imaging was halted ~10 minutes before and after perfusion of hypotonic solutions to readjust the Z-stacks.

Images from 2P experiments were processed using FIJI (Schindelin et al., 2012). Time-lapse videos were created from maximum intensity projections of sequential Z-stacks. To correct for focal or stage drift, the movies were registered using the Linear Stack Alignment with SIFT plugin as described (Lowe, 2004). Simple Neurite Tracer (Baron et al., 2014; Longair et al., 2011) and MTrack2 (Carbonell et al., 2005) plugins were used to assess the morphology and velocity of microglial processes, respectively. Morphological and velocity analysis was conducted on microglia confined to focal view (x, y, and z) for the duration of the experiment. Primary processes were defined as protrusions coming directly from the cell body; higher-order branches were differentiated by a change in thickness and orientation from a lower-order branch. Convex hull area, measured by connecting the distal terminal ends of processes is often used to approximate the area of tissue surveilled by a microglial cell (Fontainhas et al., 2011; Kongsui et al., 2014; Sołtys et al., 2001). Fluorescence intensity was determined using the GECIquant plugin in FIJI (Srinivasan et al., 2015). Time-lapse images were processed before analysis by subtracting background intensities. The spatial location of calcium transients was delineated with GECIquant's semi-automatic region of interest (ROI) detection module, with the mean fluorescence intensity computed for each ROI.

Statistics.

The data were analyzed with GraphPad Prism 9.0, with the results reported as mean ± S.E.M.. Normality was assessed with the Shapiro-Wilk test. Unless specified otherwise, an unpaired t-test was used to compare two means and ANOVA was used to compare three or more means. Multiple comparisons were performed using the Holm-Šídák or Dunnett's tests. Non-parametric data was analyzed using the Kruskal-Wallis test with Dunn's test for multiple comparisons. $p > 0.05$ = NS, $p < 0.05$ = *, $p < 0.01$ = **, $p < 0.001$ = *** and $p < 0.0001$ = ****. The data that support the findings from the study are available upon reasonable request.

Results

Retinal microglial thermoTRP transcript expression pattern is tissue-specific

We ascertained the relative expression of vanilloid "thermoTRP" genes (*Trpv1–6*) in purified mouse retinal microglia and compared expression to the expression in cortical microglia. Transcript expression in retinal microglia is dominated by *Trpv2*, showing the relative expression pattern of *Trpv2>Trpv1>>Trpv3>Trpv4>Trpv6* (Figure 1a) that differs markedly

from the pattern of expression in cortical cells (*Trpv4>Trpv6>Trpv2>Trpv3>Trpv1)*, where *Trpv4* is the dominant vanilloid *Trp* gene. With the exception of *Trpv6,* cortical microglia expressed 1.93 ± 0.47 – 13.2 ± 0.39 times more vanilloid transcripts than retinal microglia (Figure 1b). Another interesting difference concerns the relative amounts of *Trpv4* mRNA across retinal microglia, neurons, and macroglia. Microglial *Trpv4* expression showed ~3–4 fold lower levels compared to Müller cell and retinal ganglion cell (RGC) cohorts but exceeded astroglial expression (Figure 1c & d). The differences in microglial, RGC and Müller *Trpv* gene expression and the profound dissimilarities between cognate retinal and cortical cells suggest that microglial capacity for transducing mechanical, thermal and chemical cues may be region-specific, and differ from local neuronal, macroglial and endothelial sensing.

To corroborate the presence of *Trpv4* mRNA at the protein level, we tracked reporter expression in *Trpv4*^{eGFP} retinas and analyzed TRPV4 immunoreactivity in transgenic retinas in which the microglial populations were labeled by enhanced green fluorescent protein (eGFP) driven by the fractalkine promoter. In a subset of experiments, microglia were labeled by Iba1 antibodies. Dissociated CX3CR1$^{GFP/+}$ cells and RGCs (asterisk in the inset in Figure 2a) were consistently immunoreactive for TRPV4 whereas non-expressing cells (rod photoreceptors, bipolar cells) were TRPV4 immunonegative (Yarishkin et al., 2018). *Trpv4*^{eGFP} retinas (Lakk et al., 2018; Luo et al., 2018) showed prominent developmental reporter expression in cells that were immunoreactive for Iba1. eGFP^{+} Iba1^{+} cells stratified across RGC/NFL, inner plexiform, and outer plexiform layers (Figure 2b) and showed both ameboid (Figure 2c) and ramified (Figure 2d) morphologies. These data suggest that the retinal microglial TRPV4 lineage includes cells with activated and resting phenotypes.

Microglial TRPV4 activation is slow

We tested whether modest transcript/protein expression (Figure 1) suffices for functional expression of TRPV4 signals by voltage-clamping wholemount microglia and probing for agonist-induced currents. Unstimulated CX3CR1$^{GFP/+}$ cells have small steady-state inward currents and outward current measured at the holding potentials ranging from −100 mV to 100 mV; the I-V curves of the whole-cell current had the reversal potential ~ 0 mV. Exposure to the selective TRPV4 agonist GSK1016790A (GSK101, 25 nM) evoked a non-inactivating current with a time-to-peak of several minutes (Figure 3a–c) that showed inward and outward rectification. I_{TRPV4} reversed at −0.05 ± 0.03 mV (n = 6; Figure 3a) and was blocked by the selective TRPV4 antagonist HC067047 (HC-06, 2 μM) (Figure 3a–d). The resting membrane potential recorded under current-clamp conditions was −14.0 ± 5.1 mV whereas GSK101 induced significant (p = 0.001, paired t-test) −19.9 ± 5.2 mV hyperpolarizations in all cells that responded to GSK101 (4 out of 7 cells). These data demonstrate that retinal microglia express functional TRPV4 channels which activate slowly but stay open in the continued presence of the stimulus. Despite the small amplitude, TRPV4-mediated currents are associated with substantial changes in the membrane potential, presumably due to Ca^{2+}-activated K^{+} channel activation within local microdomains (e.g., Fernandez-Fernandez et al., 2008; Li et al., 2016; Sonkusare et al., 2012).

Microglial calcium signals are compartmentalized and regulate lamellipodial motility

Key microglial functions such as the production and release of cytokines require $[Ca^{2+}]_i$ elevations (Färber & Kettenmann, 2006; Hoffmann et al., 2003; Tvrdik & Kalani, 2017). To characterize microglial TRPV4 signaling in the absence of non-autonomous factors, we tested agonist- and hypotonicity (HTS)-induced responses in dissociated $CX3CR1^{GFP/+}$ retinal microglia loaded with the calcium indicator Fura-2 AM. A representative trace recorded from an individual cell is shown in Figure 4a and Supplementary Figure 1. GSK101 (25 nM; black trace) produced a sustained ~10-fold increase in $[Ca^{2+}]_i$ that was reversible upon washout and inhibited by HC-06 (red trace in Figure 4a). Averaging the peak 340/380 ratios of GSK101-evoked $[Ca^{2+}]_i$ elevations showed an increase from the 0.157 ± 0.06 baseline to 1.62 ± 0.59 (n = 8 cells, N = 3 retinas; p = 0.031) (Figure 4b). Responses in a subset of cells were calibrated to obtain information about absolute $[Ca^{2+}]_i$ in the presence/absence of GSK101, showing an increase from 103.4 ± 41.8 nM in resting cells to 892.5 ± 204.07 nM (n = 5, p = 0.011, paired t-test) in response to the agonist (Supplementary Figure 1). When studied in dissociated cells, GSK101-induced $[Ca^{2+}]_i$ elevations resulted in a remarkable cessation of microglial lamellipodial ruffling and motility that was both immediate and reversible (Video I). These data suggest that stimulation of the TRPV4 channel can lead to substantial changes in retinal microglial membrane potential, Ca^{2+} homeostasis, and cellular dynamics.

Little is known about the functional properties of surveilling CNS microglia in part because of technical difficulties inherent in studying calcium responses in unperturbed cells (Brawek & Garaschuk, 2017). This disadvantage can be obviated in the retinal wholemount preparation in which microglia preserve the morphological and functional properties of surveying cells (Fontainhas et al., 2011; Wang et al., 2016). Microglial branching and $[Ca^{2+}]_i$ changes were tracked in inner plexiform layer (IPL) of Iba1-Cre;GCaMP5-tdT cells that express the Ca^{2+} indicator GCaMP5 with the tdTomato reporter (Gee et al., 2014; Pozner et al., 2015). As shown in Video II, surveilling microglia form a stationary mosaic composed of ramified processes that probe the adjacent tissue through dynamic random extensions and retractions. Similar to cortical cells (Eichhoff et al., 2010), the rare spontaneous increases in GCaMP5 fluorescence in retinal microglial processes do not appear to correlate with process extension/retraction (Figure 4e; Video II). Exposure to HC-06 alone had no discernable effects on cell ramification, surveillance and $[Ca^{2+}]_i$ (Figure 4b,d and Supplementary Figure 2), indicating that TRPV4 is largely quiescent under isotonic conditions. Consistent with the data from dissociated cells, *in situ* applications of GSK101 evoked synchronized and sustained $[Ca^{2+}]_i$ increases across the cell bodies, primary and distal processes of intact microglia (black trace in Figure 4c). Quantification of perikaryal calcium signals (Figure 4d) showed ~3-fold increase from the baseline of 0.107 ± 0.017 to 0.308 ± 0.06 (p = 0.0008) (n = 4, N = 3 retinas), with time-lapse imaging showing an increase in the frequency of spontaneous Ca^{2+} events from 0.12 ± 0.04 to 0.31 ± 0.05 events min^{-1} (n = 8 – 19 cells, p = 0.0035, Kruskal-Wallis with Dunn's test) (Figure 4e, f). Confirming specificity, these responses were nhibited by HC-06 (0.15 ± 0.05; red trace in Figure 4c,f) (p = 0.048; n = 5). $[Ca^{2+}]_i$ signals evoked by GSK101 were associated with rapid retraction of tdT-labeled distal processes towards the cell body (Figure 4g; Video II).

Activation of microglial TRPV4 channels requires proinflammatory lipid messenger signals

The slow onset of microglial TRPV4 currents and $[Ca^{2+}]_i$ signals suggests potential involvement of intermediary mechanisms. We tested the polyunsaturated fatty acid (PUFA) mechanism shown to drive TRPV4 signaling in cortical astrocytes and retinal Müller cells (Dunn et al., 2013; Ryskamp et al., 2014) by exposing the cells to arachidonic acid, eicosanoids, and blockers of PLA2 and cytochrome P450 enzymes. Arachidonic acid (100 μM), a PUFA activator of TRPV4, elevated $[Ca^{2+}]_i$ from 0.06 ± 0.02 to 0.72 ± 0.01 ($p < 0.0001$) (black trace in Figure 5a) an effect that was suppressed by HC-06 to 0.24 ± 0.01 ($p = 0.047$, Kruskal Wallis with Dunn's test; $n = 17$) (red trace in Figure 5a & b).The residual $[Ca^{2+}]_i$ component observed in the presence of HC-06 may reflect an incomplete block at this concentration of HC-06 or stimulation of Ca^{2+}-permeable arachidonate-gated (ARC) channels (Shuttleworth, 2009). We also assessed microglial sensitivity to epoxyeicosatrienoic (EET) metabolites that represent the final common element in the TRPV4 activation pathway (Watanabe et al., 2003). Two eicosanoids, 5,6-EET and 11,12-EET, elevated $[Ca^{2+}]_i$ to 0.35 ± 0.07 ($n = 7$; $p = 0.001$, Kruskal Wallis with Dunn's test) and 0.86 ± 0.19 ($n = 44$; $p < 0.0001$, Kruskal Wallis with Dunn's test), respectively (Figure 5b,c). We conclude that microglial TRPV4 signaling requires an obligatory activation of the PLA2-CYP450 pathway, with channel activation contingent upon epoxygenation of arachidonic acid and production of EETs. The inhibition of EET-evoked $[Ca^{2+}]_i$ increases by HC-06 (5,6-EET: $p = 0.0098$; 11,12-EET: $p < 0.0001$; Kruskal Wallis with Dunn's test) demonstrates that the eicosanoid effects on $[Ca^{2+}]_i$ are mediated by TRPV4.

TRPV4 mediates the retinal microglial response to hypoosmotic swelling

Originally identified by their ability to transduce hypotonic stimuli (HTS) in recombinant cells (Strotmann et al., 2000), TRPV4 channels were subsequently shown to promote and/or regulate swelling across the body, including in a subset of macroglia (Becker et al., 2005; Hoshi et al., 2018; Jo et al., 2015; Lee et al., 2019, but see Chmelova et al., 2019). We investigated the dynamics of microglial volume regulation by treating $eGFP^+$ cells with HTS while keeping the ionic strength of the external solution constant (Jo et al., 2015; Ryskamp et al., 2011). The studies were conducted in dissociated cells because time-dependent changes in tissue volume preclude *in situ* focusing and complicate interpretation of non-ratiometric GCaMP5 fluorescence changes (Nakai et al., 2001; Schneidereit et al., 2016; Xiao et al., 2017). The Fura-2 indicator was used to track water influx across the plasma membrane by tracking its Ca^{2+}-independent fluorescence that is inversely proportional to the cell volume (e.g., Jo et al., 2015, 2016). The black trace in Figure 6a represents the response of a cell to 54% reduction in extracellular osmolality (to 140 mOsm). The time course of the hypotonicity response consisted of peak swelling (29.4 ± 2.2% increase in cell volume; Figure 6a,b) that was followed by a regulatory volume decrease (RVD). HTS-induced changes in cell volume changes were reversible, returning to original levels within 2–3 minutes upon re-addition of isotonic saline (Figure 6a). HC-06 both reduced the extent of cell volume increase (red trace in Figure 6a) and reduced the amplitude of the RVD plateau to 16.48 ± 1.97% of the original volume increase ($n = 9$; $p = 0.0006$) (Figure 6a & b). The reduction in the initial extent of cell swelling presumably reflects inhibition of glial TRPV4- and calcium-dependent mechanisms (Jo et al., 2015; Ryskamp et al., 2014); however, further studies are needed to elucidate the link between TRPV4 activation and microglial swelling.

Analysis of HTS-dependent whole-cell conductance in reporter-tagged cells showed substantial increases in inward and outward current (Figure 6c,e–f). The cells were voltage-clamped at ±100 mV and exposed to 140 mOsm, which triggered a current characterized by slow onset, outward rectification and the sensitivity to HC-06, which inhibited its inward components and reduced the outward component ($p = 0.01$, paired t-test) (Figure 6d–f), leaving a residual outward current presumably mediated by Cl^- ions (Mongin, 2015; Schlichter et al., 2011). To include the properties of cells with different morphologies, the currents in Figure 6f were normalized assuming a membrane capacitance of 1 $\mu F/cm^2$ (Boucsein et al., 2000).

TRPV4 is a nonselective cation channel with P_{Ca}/P_{Na} ~10 (White et al., 2016). To track the calcium component of channel activation, we loaded dissociated cells with Fura-2 AM and exposed them to HTS. A 5% decrease in extracellular osmolality induced modest, sustained increases in the ratio signal (Figure 7a,d) from 0.065 + 0.015 to 0.33 + 0.036 ($n = 8$, $p = 0.0091$, Dunnett's test). A further 32% decrease in tonicity, comparable to stimuli utilized in studies of microglia (Konno et al., 2012) and retinal macroglia (Jo et al., 2015) elevated $[Ca^{2+}]_i$ levels to 1.37 ± 0.068 ($n = 3$) (black trace in Figure 7a,c) whereas preincubation with HC-06 reduced the response to 0.41 ± 0.038 ($n = 20$; $p < 0.0001$, Dunnett's test; red trace in Figure 7b; Figure 7d), a ~70% reduction. CNS injury promotes formation of AA and eicosanoids (Birnie et al., 2013), which may drive glial swelling and edema in the diabetic retina (Pannicke et al., 2006). The cPLA2 antagonist p-bromophenacyl bromide (pBPB) reduced the amplitude of HTS-evoked $[Ca^{2+}]_i$ signals to 0.72 ± 0.04 ($n = 15$; $p < 0.0001$, Dunnett's test; red trace in Figure 7b; Figure 7c) whereas clotrimazole (CTZ; 10 μM), an inhibitor of cytochrome P450 (CYP450) oxidases that mediate the epoxygenation process downstream from PLA2 (Watanabe et al., 2003; White et al., 2016), resulted in partial but significant ($p < 0.0001$, Dunnett's test) suppression of HTS-induced $[Ca^{2+}]_i$ elevations (to 0.59 ± 0.02; $n = 13$) (Figure 7c). Hence, injury-induced release of polyunsaturated fatty acids (Birnie et al., 2013; Staub et al., 1994) and PLA2 activation could drive the microglial TRPV4-mediated osmoresponse via the eicosanoid messenger pathway.

Physiological osmolarity shifts modulate microglial morphology and dynamics

Microglial morphology reflects their physiological state and inflammatory status (Nimmerjahn et al., 2005), with the transition between "activated", amoeboid and "resting" surveilling phenotypes regulated by a wide range of environmental stressors (Kettenmann et al., 2011; Wolf et al., 2017). To establish the *in situ* relationship between osmotic gradients and morphology, retinas were stimulated with hypoosmolar solutions while the motility of microglial processes and perikaryal remodeling within the retinal inner plexiform layer (IPL) were monitored with time-lapse 2-photon microscopy. Epitomizing the "resting" state, unstimulated $CX3CR1^{GFP/+}$ microglia were ramified with continual distension/retraction of processes (top panel(s) of Figure 8a,b; Video III). Reduction of extracellular osmolality to 285 mOsm (~5%, equivalent to tonicity changes in patients with mild traumatic brain injury; Balak et al., 2009; Liotta et al., 2018) did cause a dramatic shift in the overall dendritic symmetry and arbor size. We observed slight perikaryal enlargement (bottom panel of Figure 8a,) and thickening of 2^{nd}- 3^{rd} order branches within an hour of exposure to the hypotonic stimulus (bottom panels of Figure 8a,b; Video III). The number of

secondary processes (protrusions extending from primary processes) was slightly but non-significantly reduced (25.9 ± 4.20) vis à vis isotonic (22.5 ± 2.01) conditions (Figure 8c; p = 0.07; two-way ANOVA), but the average process length showed no discernable differences from controls (Figure 8d). The shift in microglia towards a turgid phenotype was blocked by preadminstration of HC-06 (Figure 8c,d). Interestingly, co-administration of 285 mOsm HTS and HC-06 resulted in microglia with a significantly increased number of secondary and tertiary processes (Figure 8c) (n = 5, p = 0.02 and p < 0.04, respectively) compared to isotonic conditions. The hyper-ramification was not observed in isotonic saline with added HC-06 (Supplementary Figure 2), suggesting that hypotonic swelling triggers parallel activation of pro-branching and TRPV4-mediated branch-suppressive mechanisms. The effects were maintained for ~1 hour after return to isotonicity (data not shown), suggesting continued activation of downstream signaling mechanisms. It is thus possible that physiological changes in osmotic gradients steer quiescent microglia towards a priming phenotype that modulates their response to other environmental inputs (Sołtys et al., 2001).

Subarachnoid hemorrhage, brain tumors, TBI and cerebral edema can result in hypotonic shifts that reach below 190 mOsm (63% tonicity; Giuliani et al., 2014). A previous report suggested that TRPV4 activation in cultured cortical microglia promotes the quiescent state (Konno et al., 2012); however, historically, reports of Ca^{2+} elevations have tended to associate them with the activated state (Kettenmann et al., 2011; Tvrdik & Kalani, 2017). To gain more insight into this process, we explored how TRPV4 inhibition impacts on process dynamics observed in the presence of hypotonic stress in intact IPL microglia using ion gradients comparable to those utilized in studies of microglial (Konno et al., 2012; Schlichter et al., 2011) and retinal macroglial (Bringmann et al., 2006; Wurm et al., 2011; Jo et al., 2015) HTS signaling. We found that 190 mOsm saline results in substantial alterations in perikaryal size and branching of retinal microglia. Figure 9 illustrates that large HTS decreases ramification and promotes the retraction and/or hypertrophy of existing processes (Figure 9a,b), resulting in loss of secondary and tertiary processes (p < 0.0001, n = 22; Figure 10a) and a small, insignificant (p = 0.10, n = 22) increases in the length of primary processes (Figure 10b; Video IV). In the presence of 190 mOsm, microglia covered significantly less area (1422.7 ± 0.312 μm^2; n = 9) compared to the cells perfused with isotonic solution (2922.6 ± 261.6 μm^2; n = 13; p = 0.0029) (Figure 10c). 190 mOsm HTS significantly reduced the branching complexity but did not affect the speed at which the processes moved compared to isotonic conditions (Figure 10d, p = 0.33, Kruskal Wallis with Dunn's test).

HC-06 antagonized swelling-induced process retraction by promoting the size of secondary and tertiary branches (Figure 9c,d). Interestingly, comparison of HTS + HC-06-treated cells to isotonic controls and HC-06-only-treated cells revealed a large (115.9 ± 61.6%) and significant (p = 0.0063) increase in the average area surveyed by the dendritic tree (Figure 10c; n = 4). The length of the primary process under these conditions decreased to 20.2 ± 1.4 μm, a significant (Figure 10b, p = 0.008) change compared to hypotonicity-only stimulated cells. Moreover, in the presence of HTS + HC-06, the cells were more ramified and exhibited thinner processes that extended into the adjacent extracellular space (Figure 9c; Movie V). The average number of secondary (15.4 ± 2.08; p = 0.0003), tertiary (12.0 ± 1.03; p < 0.0001) and quaternary processes (5.75 ± 1.07; n = 4 p = 0.0071) per

microglia was increased compared to microglia treated with hypotonic stress alone without affecting the average length of the processes (Figure 10a). The motility of HC-06-pretreated processes in hypotonic solutions was faster (1.16 ± 0.58 μm/min; n = 4) compared to cells studied in control (0.83 ± 0.19 μm/min; n = 22) (p = 0.0.002, Kruskal Wallis with Dunn's test), HTS (0.74 ± 0.37 μm/min; n = 22; p < 0.0001) and HC-06 -treated cells (0.76 ± 0.17 μm/min; n = 26, p = 0.0006, Kruskal Wallis with Dunn's test) (Figure 10d). These data demonstrate that swelling-induced morphological changes in retinal microglia involve TRPV4-dependent remodeling of microglial processes, with the cells adopting several morphological characteristics of the activated state but without discernable differences in the velocity of microglial surveillance. Taken together, these data suggest that osmotic stressors will alter the Ca^{2+} homeostasis, architecture, and remodeling of CNS microglia.

Discussion

This study shows that hypoosmotic conditions regulate microglial signaling and morphology via TRPV4-mediated transduction. Our findings include: (i) TRPV4 activation mediates swelling-induced transmembrane cation fluxes and synchronized $[Ca^{2+}]_i$ elevations without impacting surveillance, (ii) Swelling-induced microglial calcium signals require availability of eicosanoid metabolites known to play roles in proinflammatory CNS signaling, (iii) TRPV4 activation correlates with branch retraction, and (iv) The distinctiveness of retinal microglial *Trpv* transcriptome relative to neuron and macroglial expression, and cortical microglia, suggests cell- and regional specificity of transduction of local sensory cues. Importantly, TRPV4-dependence of the microglial response to small osmolality gradients suggests sensitivity to activity-dependent physiological signaling within the retina.

Trpv4 mRNA expression in adult retinal microglia was congruent with antibody staining, reporter signals, and functional measurements, with expression consistently observed in dissociated, intact and *Trpv4*^{eGFP} cells. The presence of $TRPV4^{eGFP}$ reporter molecules and physiological responses in ramified and amoeboid cells suggest that TRPV4 signaling extends across activation states. RNA profiling showed *Trpv4* transcript levels in microglia to be 3–5-fold lower compared to RGC and Müller glial signals whereas comparison of *Trpv* signals in retina vs. cortex identified the major retinal vanilloid transcript to be *Trpv2* vs. *Trpv4* in the cortical cohort. Thus, retinal but not cortical microglial *Trpv4* expression trails the levels of cognate *Trpv1*-2 genes that encode proteins sensitive to temperature, endogenous lipids, osmotic and mechanical stressors. Our analysis of *Trpv* signals is consistent with the data from the Barres lab RNASeq database (Zhang et al., 2014) and with recent indications that microglial transduction of biomechanical and chemical cues differs across the CNS (Bennet et al., 2018; De Biase et al., 2017; Hickmann et al., 2013; Silvin and Ginhoux, 2018). Low levels of retinal microglial *Trpv4* expression relative to RGCs, Müller glia and astrocytes, and relative to cortical microglia, oligodendrocytes, endothelial cells and neurons (Figure 1) (Zhang et al., 2014), might reflect the specifics of respective biomechanical milieus. For example, modest expression in the retina may suffice to subserve microglial sensing of physiological osmotic/mechanical cues (5% decrease in tonicity) without triggering the proinflammatory pathways. It is possible that intracellular signaling amplification (Figure 5) (Toft-Bertelsen et al, 2019) that underlies branch retraction and proinflammatory-like phenotypes in cells stimulated with GSK101 and moderate swelling

(Figures 4 & 9), overrides the protective effects of modest expression during edema and/or ocular hypertension. We recently observed that TRPV4 can be activated by low levels of pressure-induced membrane strain (Lakk and Krizaj, 2020; Yarishkin et al., 2020) and cyclic stretch (Ryskamp et al., 2016) which might contribute to microglial activation by relatively mild increases in IOP (~5 mm Hg) (Howell et al., 2007; Bosco et al., 2011).

The low resting conductance and $[Ca^{2+}]_i$ levels in unstimulated microglia suggest that small ionic fluxes could have an outsize influence on the membrane potential and $[Ca^{2+}]_i$. The lack of HC-06 effect on $[Ca^{2+}]_i$, V_{rest} and branching in isotonic cells at room temperature indicates that TRPV4 does not mediate the constitutive cation influx that helps set the microglial resting potential at relatively depolarized levels (Izquierdo et al., 2019) but it remains to be seen whether its contribution increases at body temperature (Shibasaki, 2020). The quasi-linear I-V relationship evoked by GSK101 and HTS suggests an absence of major TRPV4-dependent inwardly- and outwardly rectifying potassium conductances in ramified microglia. On the other hand, the substantial hyperpolarizations seen under current clamp in cells stimulated with GSK101 suggest activation of Ca^{2+}-dependent mechanisms that remain to be identified.

The outward rectification of the TRPV4-mediated current that we observe in microglia recalls the properties of homomeric TRPV4 channels in recombinant HEK293 cells, retinal microvascular cells, Müller cells and trabecular meshwork cells (Ryskamp et al., 2016; Phuong et al., 2017; Lakk et al., 2017; Watanabe et al., 2003) whereas TRPV4 overexpressing oocytes show linear I-V relationships (Toft-Bertelson et al., 2017). Similar to endothelial cells (Li et al., 2016; Sonkusare et al., 2012; White et al., 2016), (~5 – 10 mV) hyperpolarizations induced by TRPV4 activation might reflect microdomain coupling with Ca^{2+}-activated K^+ conductances. However, TRPV4 activation, kinetics and time course are cell type-dependent (Toft-Bertelsen et al., 2019), potentially due to the association with modulatory proteins (e.g., PAR2, PACSIN3, STIM1, AIP4), phosphorylation (PKA, PKC, Src kinases), availability of phosphatidylinositol 4,5-biphosphate (D'Hoedt et al., 2008; Grant et al., 2007) and/or presence of splice variants (White et al., 2016).

Calcium signaling is a central, yet incompletely understood, feature of microglial biology (Kettenman et al., 2011; Brawek & Garaschuk, 2017). Because reactivity tends to correlate with increased $[Ca^{2+}]_i$ (Hoffmann et al., 2003; Tvrdik & Kalani, 2017), process retraction observed in Iba1-GCaMP5 cells stimulated with GSK101 (Figure 4) suggests a potential trigger mechanism for cell activation in the presence of mechanical stress. Interestingly, while retinal microglia responded to TRPV4 agonism and HTS stimuli with branch retraction and hyperpolarization, cultured cortical microglia showed the opposite response as the agonist 4α-PDD depolarized the cells and promoted ramification (Konno et al., 2012). The discrepancy could reflect differential channel expression in the retina vs. cortex (e.g., Figure 1), heteromerization, or altered electrophysiological properties in cultured cells (Butovsky et al., 2014; Kloss et al., 1997; Madry et al., 2018; Morihata et al., 2000).

Data from isolated cells and intact retinas show that TRPV4 activation is associated with inward currents, calcium signals, hyperpolarization and lamellipodial ruffling. We found microglial morphology to be subtly altered by small (~5%) hypotonic gradients (Figure

8), whereas additional osmolality stress shifted the balance of primary vs. higher-order processes towards increasingly dystrophic phenotypes that might be considered a graded form of cell activation. Indicating obligatory TRPV4 activation, HTS-evoked changes in ramification were mimicked by GSK101 (Figure 4) and suppressed by HC-06 (Figures 8–10). It is possible that retraction of higher-order branches "primes" microglia to respond more vigorously to other pathological stressors (Hoeijmakers et al., 2016) as reported for inflammatory states associated with mechanical allodynia, joint inflammation, diabetes and pulmonary fibrosis (Alessandri-Haber et al., 2003; Bourinet et al., 2014; Scheraga et al., 2017; Ye et al., 2012). In mice, portal vein osmolality dropped by 8% following oral water intake (Lechner et al., 2011) and it seems conceivable that the local retinal milieu under pathological circumstances such as edema is associated with significant osmogradients (Pannicke et al., 2006).

While our results in isolated cells (Figures 4a,b & 7) and *ex vivo* retinas (Figure 4c, d) link TRPV4 activation to cation influx and $[Ca^{2+}]_i$ elevations, and we find that TRPV4 inhibition suppresses swelling-induced branch retraction in intact retinas (Figures 8 & 10), our experiments cannot exclude potential contributions from non-autonomous TRPV4-dependent mechanisms. GSK101- and HTS-induced retraction of microglial processes argues against a primary role for P2Y12 receptors, which tend to promote branching and surveillance (Fontainhas et al., 2011; Kettenman et al., 2011). Adenosine, acting via A2A receptors was shown to induce microglial retraction during inflammatory states but had less effect on ramified microglia in the healthy brain (Orr et al., 2009). The remarkable increase in the number of secondary and tertiary processes in cells exposed to physiological (5%) HTS in the presence of HC-06 (Figures 8 & 10) suggests that hypoosmotic stress induces TRPV4-dependent suppression of branching (unmasked by HC-06) in parallel with an unknown pro-branching pathway that could involve local ATP release. In future studies, the molecular mechanisms that mediate volume-dependent branch extension and retraction should be clarified with cell-type specific mouse knockout lines. In any case, our data suggest that inhibition of retinal TRPV4 channels profoundly affects microglial morphology, potentially impeding the transition towards proinflammatory-like phenotypes in tissues exposed to hypotonic gradients (e.g., Chmelova et al., 2019; Gankam-Kengne et al. 2010).

Hypotonicity-induced swelling of isolated microglia was sensitive to TRPV4 inhibition, with HC-06 reducing the magnitude of the volume decrease together with decreases in membrane current and $[Ca^{2+}]_i$ (Figure 6). These observations suggests that TRPV4-mediated cation entry is coupled to transmembrane water flux, as reported for Müller glia, which respond to TRPV4 activation with increases in cell volume that are inhibited by HC-06, *Trpv4* knockdown and BAPTA-AM (Jo et al., 2015). Astrocytes similarly respond to the TRPV4 agonist arachidonic acid with augmented swelling (Basavappa et al., 1998; Birnie et al., 2013; Chan et al., 1983; Pannicke et al., 2006; Staub et al., 1994), suggesting a potential role for swelling-induced PLA2 activation (Lambert et al., 2006). It remains to be seen whether, as shown for macroglia and heterologous cell models (Jo et al., 2015; Mola et al., 2016; Toft-Bertelsen et al., 2017; 2019), microglial TRPV4 activation is functionally coupled to aquaporin channels and/or Ca^{2+}-dependent ionic fluxes (Stokum et al., 2018). Hypotonicity, TRPV4 activation and ATP-evoked $[Ca^{2+}]_i$ increases did not significantly impact on *in situ*

microglial surveillance, which instead may respond to K^+ gradients (Madry et al., 2018). While the relationship between motility and calcium is likely complex (Lanfelder et al., 2015; Umpierre et al., 2020), we previously observed that chelating microglial calcium reduces process velocity without abolishing motility (Pozner et al., 2015). The suppression of lamellipodial ruffling by GSK101 (Video I) and the TRPV1 agonist capsaicin (S.N.R. and D.K., unpublished observations) suggests that swelling-induced and TRP-mediated Ca^{2+} influx could influence at least some forms of microglial motility, possibly via microdomain interactions with cAMP and/or PI3 kinase pathways (Zierler et al., 2008; Bernier et al., 2019; Cianculli et al., 2020) and integrin-β1/β3 -based contacts which bind TRPV4 (Matthews et al., 2010) and mediate stretch-dependent remodeling of focal adhesions (Lakk and Krizaj, 2020).

A broad implication of our findings is that retinal microglia are sensitive to the mechanical microenvironment, with direct inhibition of intrinsic TRPV4 channels and TRPV4-dependent signaling within neuronal-glial circuits as a viable strategy to counter the proinflammatory sequelae of the excessive movement of water and mechanical trauma. Swelling is a conserved danger signal across the vertebrate kingdom (Hoffmann et al., 2009), especially in immune cells, which respond to decreased osmolarity with Ca^{2+} influx through stretch-activated TRP channels, production of eicosanoid messengers and stimulation of downstream inflammatory pathways (the NLRP3 inflammasome, TAK1 kinases, and IL-1β release; Compan et al., 2012). Consistent with its key role in osmosensation (Toft-Bertelsen et al., 2017), the $TRPV4_{P19S}$ N-terminal mutation has been associated with hyponatremia and reduced responsiveness to moderate (15%) HTS and EETs (Tian et al., 2009). Accumulation of cellular metabolites during ischemia/reperfusion leads to >40% increase in cell volume (Wright and Rees, 1997) and stimulation of PLA2 (Lambert et al., 2006), which has been implicated in pathological swelling, loss of barrier integrity (Pannicke et al., 2006), and activation of macroglial (Ryskamp et al., 2014; Toft-Bertelsen et al., 2019) and microglial (Figure 5) TRPV4 channels. Our finding that HC-06 reduces HTS-induced swelling is consistent with inhibition of swelling (Pannnicke et al., 2006; Ryskamp et al., 2014), and reduced lung/brain edema formation followed treatment with TRPV4 and PLA2 antagonists (Balakrishna et al., 2014; Hoshi et al., 2018; Thorneloe et al., 2012; Zhao et al., 2018). Moreover, rodent $TRPV4^{-/-}$ tissues appear to be protected against many thermal, mechanical, ischemic and inflammatory insults (Alessandri-Haber et al., 2006; Ryskamp et al., 2014a; Ye et al., 2012) that include CNS edema (Pivonkova et al., 2018; Hoshi et al., 2018; Shibasaki, 2020). Targeting the TRPV4 - PLA2 – eicosanoid axis might have beneficial effects in treatments of edema, spreading depression, epileptiform activity and proinflammatory signaling in tissues exposed to pathological osmotic gradients.

Supplementary Material

Refer to Web version on PubMed Central for supplementary material.

ACKNOWLEDGEMENTS:

Supported by the National Institutes of Health (R01EY022076, R01EY027920; P30EY014800), Willard L. Eccles Foundation, Glaucoma Research Foundation, ALSAM-Skaggs Foundation, University of Utah Neuroscience Initiative and unrestricted support from Research to Prevent Blindness to the Moran Eye Institute at the University

of Utah. We thank Dr. Wolfgang Liedtke for TRPV4$^{-/-}$ mice, Dr. Naveen Nagarajan for CX3CR1^{eGFP} mice and Dr. Honghzhen Hu for the TRPV4^{eGFP} mice.

References

Alessandri-Haber N, Yeh JJ, Boyd AE, Parada CA, Chen X, Reichling DB, & Levine JD (2003). Hypotonicity induces TRPV4-mediated nociception in rat. Neuron, 39(3), 497–511. doi: 10.1016/s0896-6273(03)00462-8 [PubMed: 12895423]

Alessandri-Haber N, Dina OA, Joseph EK, Reichling D, Levine JD (2006). A transient receptor potential vanilloid 4-dependent mechanism of hyperalgesia is engaged by concerted action of inflammatory mediators. The Journal of Neuroscience, 26(14), 3864–3874. doi: 10.1523/jneurosci.5385-05.2006 [PubMed: 16597741]

Arcuri C, Mecca C, Bianchi R, Giambanco I, & Donato R (2017). The pathophysiological role of microglia in dynamic surveillance, phagocytosis and structural remodeling of the developing CNS. Frontiers in Molecular Neuroscience, 10, 191. doi: 10.3389/fnmol.2017.00191 [PubMed: 28674485]

Balak N, Isiksacan N, & Turkoglu R (2009). Does serum osmolarity change as a result of the reflex neuroprotective mechanism of cerebral osmo-regulation after minor head trauma? Journal of Korean Neurosurgical Society, 45(3), 151–156. doi: 10.3340/jkns.2009.45.3.151 [PubMed: 19352476]

Balakrishna S, Song W, Achanta S, Doran SF, Liu B, Kaelberer MM, … Jordt S-E (2014). TRPV4 inhibition counteracts edema and inflammation and improves pulmonary function and oxygen saturation in chemically induced acute lung injury. American Journal of Physiology-Lung Cellular and Molecular Physiology, 307(2), L158–L172. doi: 10.1152/ajplung.00065.2014 [PubMed: 24838754]

Baron R, Babcock AA, Nemirovsky A, Finsen B, & Monsonego A (2014). Accelerated microglial pathology is associated with Aβ plaques in mouse models of Alzheimers disease. Aging Cell, 13(4), 584–595. doi: 10.1111/acel.12210 [PubMed: 24641683]

Basavappa S, Pedersen SF, Jørgensen NK, Ellory JC, & Hoffmann EK (1998). Swelling-induced arachidonic acid release via the 85-kDa cPLA2 in human neuroblastoma cells. Journal of Neurophysiology, 79(3), 1441–1449. doi: 10.1152/jn.1998.79.3.1441 [PubMed: 9497423]

Becker D, Blasé C, Bereiter-Hahn J, & Jendrach M (2005). TRPV4 exhibits a functional role in cell-volume regulation. Journal of Cell Science, 118(11), 2435–2440. doi: 10.1242/jcs.02372 [PubMed: 15923656]

Bennett FC, Bennett ML, Yaqoob F, Mulinyawe SB, Grant GA, Gephart MH, … Barres BA (2018). A combination of ontogeny and CNS environment establishes microglial identity. Neuron, 98(6), 1170–1183.e8. doi: 10.1016/j.neuron.2018.05.014 [PubMed: 29861285]

Bernier L, Bohlen CJ, York EM, Choi HB, Kamyabi A, Dissing-Olesen L, … MacVicar BA (2019). Nanoscale surveillance of the brain by microglia via cAMP-regualted filopodia. Cell Reports, 27(10), 2895–2908.e4. doi: 10.1016/j.celrep.2019.05.010 [PubMed: 31167136]

Birnie M, Morrison R, Camara R, & Strauss KI (2013). Temporal changes of cytochrome P450 (Cyp) and eicosanoid-related gene expression in the rat brain after traumatic brain injury. BMC Genomics, 14, 303. doi: 10.1186/1471-2164-14-303 [PubMed: 23642095]

Boucsein C, Kettenmann H, & Nolte C (2000). Electrophysiological properties of microglial cells in normal and pathologic rat brain slices. European Journal of Neuroscience, 12(6), 2049–2058. doi: 10.1046/j.1460-9568.2000.00100.x

Bourinet E, Altier C, Hildebrand ME, Trang T, Salter MW, & Zamponi GW (2014). Calcium-permeable ion channels in pain signaling. Physiological Reviews, 94(1), 81–140. doi: 10.1152/physrev.00023.2013 [PubMed: 24382884]

Brawek B, & Garaschuk O (2017). Monitoring in vivo function of cortical microglia. Cell Calcium, 64, 109–117. doi: 10.1016/j.ceca.2017.02.011 [PubMed: 28359543]

Bringmann A, Reichenbach A, & Wiedemann P (2004). Pathomechanisms of cystoid macular edema. Ophthalmic Research, 36(5), 241–249. Doi: 10.1159/000081203 [PubMed: 15583429]

Bringmann A, Pannicke T, Grosche J, Francke M, Wiedemann P, Skatchkov SN, … Reichenbach A (2006). Müller cells in the healthy and diseased retina. Progress in Retinal Eye Research, 25(4), 397–424. doi: 10.1016/j.preteyeres.2006.05.003 [PubMed: 16839797]

Butovsky O, Jedrychowski MP, Moore CS, Cialic R, Lanser AJ, Gabriely G, … Weiner HL (2013). Identification of a unique TGF-β–dependent molecular and functional signature in microglia. Nature Neuroscience, 17(1), 131–143. doi: 10.1038/nn.3599 [PubMed: 24316888]

Carbonell WS, Murase S, Horwitz AF, & Mandell JW (2005). Migration of perilesional microglia after focal brain injury and modulation by CC chemokine receptor 5: An in situ time-lapse confocal imaging study. The Journal of Neuroscience, 25(30), 7040–7047. doi: 10.1523/jneurosci.5171-04.2005 [PubMed: 16049180]

Chan PH, Fishman RA, Caronna J, Schmidley JW, Prioleau G, & Lee J (1983). Induction of brain edema following intracerebral injection of arachidonic acid. Annals of Neurology, 13(6), 625–632. doi: 10.1002/ana.410130608 [PubMed: 6309072]

Chiavaroli C, Bird G, & Putney JW (1994). Delayed “all-or-none” activation of inositol 1,4,5-trisphosphate-dependent calcium signaling in single rat hepatocytes. Journal of Biological Chemistry, 269(41), 25570–25575.

Chmelova M, Sucha P, Bochin M, Vorisek I, Pivonkova H, Hermanova Z, … Vargova L (2019). The role of aquaporin-4 and transient receptor potential vaniloid isoform 4 channels in the development of cytotoxic edema and associated extracellular diffusion parameter changes. European Journal of Neuroscience, 50(1), 1685–1699. doi: 10.1111/ejn.14338

Cianciulli A, Porro C, Calvello R, Trotta T, Lofrumento DD, & Panaro MA (2020). Microglia mediated neuroinflammation: Focus on PI3K modulation. Biomolecules, 10(1), 137. doi: 10.3390/biom10010137

Compan V, Baroja-Mazo A, López-Castejón G, Gomez AI, Martínez CM, Angosto D, … Pelegrín P (2012). Cell volume regulation modulates NLRP3 inflammasome activation. Immunity, 37(3), 487–500. doi: 10.1016/j.immuni.2012.06.013 [PubMed: 22981536]

D’hoedt D, Owsianik G, Prenen J, Cuajungco MP, Grimm C, Heller S, … Nilius B (2008). Stimulus-specific modulation of the cation channel TRPV4 by PACSIN 3. Journal of Biological Chemistry, 283(10), 6272–6280. doi: 10.1074/jbc.m706386200

Daruich A, Matet A, Moulin A, Kowalczuk L, Nicolas M, Sellam A, … Behar-Cohen F (2018). Mechanisms of macular edema: Beyond the surface. Progress in Retinal and Eye Research, 63, 20–68. doi: 10.1016/j.preteyeres.2017.10.006 [PubMed: 29126927]

De Biase LM, Schuebel KE, Fusfeld ZH, Jair KA, Hawes IA, Cimbro R, … Bonci A (2017). Local cues establish and maintain region-specific phenotypes of basal ganglia microglia. Neuron, 95(2), 341–356.e6. doi: 10.1016/j.neuron.2017.06.020 [PubMed: 28689984]

Diaz-Otero JM, Yen T-C, Fisher C, Bota D, Jackson WF, & Dorrance AM (2018). Mineralocorticoid receptor antagonism improves parenchymal arteriole dilation via a TRPV4-dependent mechanism and prevents cognitive dysfunction in hypertension. American Journal of Physiology-Heart and Circulatory Physiology, 315(5), H1304–H1315. doi: 10.1152/ajpheart.00207.2018 [PubMed: 30118343]

Dmitriev A, Govardovskii V, Schwahn H, & Steinberg R (1999). Light-induced changes of extracellular ions and volume in the isolated chick retina–pigment epithelium preparation. Visual Neuroscience, 16(6), 1157–1167. doi: 10.1017/s095252389916615x [PubMed: 10614595]

Donkin JJ, & Vink R (2010). Mechanisms of cerebral edema in traumatic brain injury: therapeutic developments. Current Opinion in Neurology, 23(3), 293–299. doi: 10.1097/wco.0b013e328337f451 [PubMed: 20168229]

Dunn KM, Hill-Eubanks DC, Liedtke WB, & Nelson MT (2013). TRPV4 channels stimulate Ca2+ -induced Ca2+ release in astrocytic endfeet and amplify neurovascular coupling responses. Proceedings of the National Academy of Sciences, 110(15), 6157–6162. doi: 10.1073/pnas.1216514110

Eichhoff G, Brawek B, & Garaschuk O (2011). Microglial calcium signal acts as a rapid sensor of single neuron damage in vivo. Biochimica et biophysica acta, 1813(5), 1014–1024. doi: 10.1016/j.bbamcr.2010.10.018 [PubMed: 21056596]

Färber K, & Kettenmann H (2006). Functional role of calcium signals for microglial function. Glia, 54(7), 656–665. doi: 10.1002/glia.20412 [PubMed: 17006894]

Fernández-Fernández JM, Andrade YN, Arniges M, Fernandes J, Plata C, Rubio-Moscardo F, … Valverde MA (2008). Functional coupling of TRPV4 cationic channel and large conductance,

calcium-dependent potassium channel in human bronchial epithelial cell lines. Pflügers Archiv - European Journal of Physiology, 457(1), 149–159. doi: 10.1007/s00424-008-0516-3 [PubMed: 18458941]

Fontainhas AM, Wang M, Liang KJ, Chen S, Mettu P, Damani M, … Wong WT (2011). Microglial morphology and dynamic behavior is regulated by ionotropic glutamatergic and GABAergic neurotransmission. PLoS ONE, 6(1), e15973. doi: 10.1371/journal.pone.0015973 [PubMed: 21283568]

Gankam-Kengne F, Soupart A, Pochet R, Brion JP, & Decaux G (2010). Minocycline protects against neurologic complications of rapid correction of hyponatremia. Journal of the American Society of Nephrology, 21(12), 2099–2108. doi: 10.1681/asn.2010050467 [PubMed: 21051736]

Gardner TW, Antonetti DA, Barber AJ, LaNoue KF, & Levison SW (2002). Diabetic retinopathy: More than meets the eye. Survey of Ophthalmology, 47, S253–S262. doi: 10.1016/s0039-6257(02)00387-9 [PubMed: 12507627]

Gee JM, Smith NA, Fernandez FR, Economo MN, Brunert D, Rothermel M, … Tvrdik P (2014). Imaging activity in neurons and glia with a Polr2a-based and cre-dependent GCaMP5G-IRES-tdTomato reporter mouse. Neuron, 83(5), 1058–1072. doi: 10.1016/j.neuron.2014.07.024 [PubMed: 25155958]

Giuliani C, & Peri A (2014). Effects of hyponatremia on the brain. Journal of Clinical Medicine, 3(4), 1163–1177. doi: 10.3390/jcm3041163 [PubMed: 26237597]

Gong Y, Hua Y, Keep RF, Hoff JT, & Xi G (2004). Intracerebral hemorrhage: Effects of aging on brain edema and neurological deficits. Stroke, 35(11), 2571–2575. doi: 10.1161/01.str.0000145485.67827.d0 [PubMed: 15472083]

Grant AD, Cottrell GS, Amadesi S, Trevisani M, Nicoletti P, Materazzi S, … Bunnett NW (2007). Protease-activated receptor 2 sensitizes the transient receptor potential vanilloid 4 ion channel to cause mechanical hyperalgesia in mice. The Journal of Physiology, 578(3), 715–733. doi: 10.1113/jphysiol.2006.121111 [PubMed: 17124270]

Gu QD, Moss CR 2nd, Kettelhut KL, Gilbert CA, & Hu H (2016). Activation of TRPV4 regulates respiration through indirect activation of bronchopulmonary sensory neurons. Frontiers in Physiology, 7, 65. doi: 10.3389/fphys.2016.00065 [PubMed: 26973533]

Henry CO, Dalloneau E, Pérez-Berezo M-T, Plata C, Wu Y, Guillon A, … Si-Tahar M (2016). In vitro and in vivo evidence for an inflammatory role of the calcium channel TRPV4 in lung epithelium: Potential involvement in cystic fibrosis. American Journal of Physiology-Lung Cellular and Molecular Physiology, 311(3), L664–L675. doi: 10.1152/ajplung.00442.2015 [PubMed: 27496898]

Hermoso M, Olivero P, Torres R, Riveros A, Quest AFG, & Stutzin A (2004). Cell volume regulation in response to hypotonicity is impaired in HeLa cells expressing a protein kinase C α mutant lacking kinase activity. Journal of Biological Chemistry, 279(17), 17681–17689. doi: 10.1074/jbc.m304506200

Hickman SE, Kingery ND, Ohsumi TK, Borowsky ML, Wang L-C, Means TK, & Khoury JE (2013). The microglial sensome revealed by direct RNA sequencing. Nature Neuroscience, 16(12), 1896–1905. doi: 10.1038/nn.3554 [PubMed: 24162652]

Hoeijmakers L, Heinen Y, Dam A-MV, Lucassen PJ, & Korosi A (2016). Microglial priming and Alzheimer's disease: A possible role for (early) immune challenges and epigenetics? Frontiers in Human Neuroscience, 10, 398. doi: 10.3389/fnhum.2016.00398 [PubMed: 27555812]

Hoffmann A, Kann O, Ohlemeyer C, Hanisch U-K, & Kettenmann H (2003). Elevation of basal intracellular calcium as a central element in the activation of brain macrophages (microglia): Suppression of receptor-evoked calcium signaling and control of release function. The Journal of Neuroscience, 23(11), 4410–4419. doi: 10.1523/jneurosci.23-11-04410.2003 [PubMed: 12805281]

Hoffmann EK, Lambert IH, & Pedersen SF (2009). Physiology of cell volume regulation in vertebrates. Physiological Reviews, 89(1), 193–277. doi: 10.1152/physrev.00037.2007 [PubMed: 19126758]

Hollborn M, Francke M, Iandiev I, Bühner E, Foja C, Kohen L, … Uhlmann S (2008). Early activation of inflammation- and immune response-related genes after experimental detachment of the porcine retina. Investigative Ophthalmology & Visual Science, 49(3), 1262–1273. doi: 10.1167/iovs.07-0879 [PubMed: 18326757]

Hoshi Y, Okabe K, Shibasaki K, Funatsu T, Matsuki N, Ikegaya Y, & Koyama R (2018). Ischemic brain injury leads to brain edema via hyperthermia-induced TRPV4 activation. The Journal of Neuroscience, 38(25), 5700–5709. doi: 10.1523/jneurosci.2888-17.2018 [PubMed: 29793978]

Howell GR, Libby RT, Jakobs TC, Smith RS, Phalan FC, Barter JW, … John SWM (2007). Axons of retinal ganglion cells are insulted in the optic nerve early in DBA/2J glaucoma. Journal of Cell Biology, 179(7), 1523–1537. doi: 10.1083/jcb.200706181

Izquierdo P, Attwell D, & Madry C (2019). Ion channels and receptors as determinants of microglial function. Trends in Nuerosicence, 42(4), 278–292. doi: 10.1016/j.tins.2018.12.007

Jiang W, Desjardins P, & Butterworth RF (2009). Cerebral inflammation contributes to encephalopathy and brain edema in acute liver failure: Protective effect of minocycline. Journal of Neurochemistry, 109(2), 485–493. doi: 10.1111/j.1471-4159.2009.05981.x [PubMed: 19220703]

Jo AO, Ryskamp DA, Phuong TTT, Verkman AS, Yarishkin O, Macaulay N, & Križaj D (2015). TRPV4 and AQP4 channels synergistically regulate cell volume and calcium homeostasis in retinal Müller Glia. The Journal of Neuroscience, 35(39), 13525–13537. doi: 10.1523/jneurosci.1987-15.2015 [PubMed: 26424896]

Jo AO, Lakk M, Frye AM, Phuong TTT, Redmon SN, Roberts R, … Križaj D (2016). Differential volume regulation and calcium signaling in two ciliary body cell types is subserved by TRPV4 channels. Proceedings of the National Academy of Sciences, 113(14), 3885–3890. doi: 10.1073/pnas.1515895113

Kettenmann H, Hanisch U-K, Noda M, & Verkhratsky A (2011). Physiology of microglia. Physiological Reviews, 91(2), 461–553. doi: 10.1152/physrev.00011.2010 [PubMed: 21527731]

Kim C, Cho E, Kim H, You s. Lee H, Hwang D, & Lee S (2014). β-integrin-dependent micgration of microglia in response to neuron-released α-synuclein. Experimental & Molecular Medicine, 46(4), e91. doi: 10.1038/emm.2014.6 [PubMed: 24743837]

Kimelberg HK (2005). Astrocytic swelling in cerebral ischemia as a possible cause of injury and target for therapy. Glia, 50(4), 389–397. doi: 10.1002/glia.20174 [PubMed: 15846797]

Kloss CU, Kreutzberg GW, & Raivich G (1997). Proliferation of ramified microglia on an astrocyte monolayer: Characterization of stimulatory and inhibitory cytokines. Journal of Neuroscience Research, 49(2), 248–254. [PubMed: 9272647]

Kongsui R, Beynon SB, Johnson SJ, & Walker FR (2014). Quantitative assessment of microglial morphology and density reveals remarkable consistency in the distribution and morphology of cells within the healthy prefrontal cortex of the rat. Journal of Neuroinflammation, 11, 182. doi: 10.1186/s12974-014-0182-7 [PubMed: 25343964]

Konno M, Shirakawa H, Iida S, Sakimoto S, Matsutani I, Miyake T, … Kaneko S (2012). Stimulation of transient receptor potential vanilloid 4 channel suppresses abnormal activation of microglia induced by lipopolysaccharide. Glia, 60(5), 761–770. doi: 10.1002/glia.22306 [PubMed: 22331560]

Krizaj D, Rice ME, Wardle RA, & Nicholson C (1996). Water compartmentalization and extracellular tortuosity after osmotic changes in cerebellum of Trachemys scripta. The Journal of Physiology, 492(3), 887–896. doi: 10.1113/jphysiol.1996.sp021354 [PubMed: 8734998]

Krizaj D, & Copenhagen DR (1998). Compartmentalization of calcium extrusion mechanisms in the outer and inner segments of photoreceptors. Neuron, 21(1), 249–256. doi: 10.1016/s0896-6273(00)80531-0 [PubMed: 9697868]

Krizaj D, Bao J, Schmitz Y, Witkovsky P & Copenhagen DR (1999). Caffeine-sensitive calcium stores regulate synaptic transmission from retinal rod photoreceptors. Journal of Neuroscience, 19(17), 7249–7261. doi: 10.1523/JNEUROSCI.19-17-07249.1999 [PubMed: 10460231]

Križaj D, Ryskamp DA, Tian N, Tezel G, Mitchell CH, Slepak VZ, & Shestopalov VI (2014). From mechanosensitivity to inflammatory responses: new players in the pathology of glaucoma. Current Eye Research, 39(2), 105–119. doi: 10.3109/02713683.2013.836541 [PubMed: 24144321]

Krizaj D (2019). What is glaucoma? In Kolb H, Fernandez E, & Nelson R, (Eds.), Webvision: The organization of the retina and visual system [Internet]. University of Utah Health Sciences Center.

Lakk M, Yarishkin O, Baumann JM, Iuso A, & Križaj D (2017). Cholesterol regulates polymodal sensory transduction in Müller glia. Glia, 65(12), 2038–2050. doi: 10.1002/glia.23213 [PubMed: 28856727]

Lakk M, Vazquez-Chona F, Yarishkin O, & Križaj D (2018). Dyslipidemia modulates Müller glial sensing and transduction of ambient information. Neural Regeneration Research, 13(2), 207–210. doi: 10.4103/1673-5374.226383 [PubMed: 29557361]

Lakk M, & Krizaj D (2020). Mechanically induced cytoskeletal remodeling in trabecular meshwork cells requires TRPV4 – Rho signaling interactions. bioRxiv 10.1101/2020.08.11.247171

Lambert IH, Pedersen SF, & Poulsen KA (2006). Activation of PLA_2 isoforms by cell swelling and ischaemia/hypoxia. Acta Physiologica, 187(1–2), 75–85. Doi: 10.1111/j.1748-1716.2006.01557.x [PubMed: 16734744]

Langfelder A, Okonji E, Deca D, Wei W, & Glitsch MD (2015). Extracellular acidosis impairs P2Y receptor-mediated Ca(2+) signalling and migration of microglia. Cell Calcium, 57(4), 247–256. doi: 10.1016/j.ceca.2015.01.004 [PubMed: 25623949]

Lee H-P, Stowers R, & Chaudhuri O (2019). Volume expansion and TRPV4 activation regulate stem cell fate in three-dimensional microenvironments. Nature Communications, 10(1), 529. doi: 10.1038/s41467-019-08465-x

Lee JE, Liang KJ, Fariss RN, & Wong WT (2008). Ex vivo dynamic imaging of retinal microglia using time-lapse confocal microscopy. Investigative Ophthalmology & Visual Science, 49(9), 4169–4176. doi: 10.1167/iovs.08-2076 [PubMed: 18487378]

Li Y, Hu H, Butterworth MB, Tian J-B, Zhu MX, & O'Neil RG (2016). Expression of a diverse array of Ca2+-activated K+ channels (SK1/3, IK1, BK) that functionally couple to the mechanosensitive TRPV4 channel in the collecting duct system of kidney. Plos One, 11(5), e0155006. doi: 10.1371/journal.pone.0155006 [PubMed: 27159616]

Liotta EM, Romanova AL, Lizza BD, Rasmussen-Torvik LJ, Kim M, Francis B, … Maas MB (2018). Osmotic shifts, cerebral edema, and neurologic deterioration in severe hepatic encephalopathy. Critical Care Medicine, 46(2), 280–289. doi: 10.1097/ccm.0000000000002831 [PubMed: 29341965]

Longair MH, Baker DA, & Armstrong JD (2011). Simple neurite tracer: Open source software for reconstruction, visualization and analysis of neuronal processes. Bioinformatics, 27(17), 2453–2454. doi: 10.1093/bioinformatics/btr390 [PubMed: 21727141]

Lowe DG (2004). Distinctive image features from scale-invariant keypoints. International Journal of Computer Vision, 60(2), 91–110. doi: 10.1023/b:visi.0000029664.99615.94

Luo J, Feng J, Yu G, Yang P, Mack MR, Du J, … Hu H (2018). Transient receptor potential vanilloid 4–expressing macrophages and keratinocytes contribute differentially to allergic and nonallergic chronic itch. Journal of Allergy and Clinical Immunology, 141(2), 608–619.e7. doi: 10.1016/j.jaci.2017.05.051

Madry C, Kyrargyri V, Arancibia-Cárcamo IL, Jolivet R, Kohsaka S, Bryan RM, & Attwell D (2018). Microglial ramification, surveillance, and interleukin-1β release are regulated by the two-pore domain K channel THIK-1. Neuron, 97(2), 299–312.e6. doi: 10.1016/j.neuron.2017.12.002 [PubMed: 29290552]

Marker DF, Tremblay M-E, Lu S-M, Majewska AK, & Gelbard HA (2010). A thin-skull window technique for chronic two-photon imaging of murine microglia in models of neuroinflammation. Journal of Visualized Experiments, (43), 2059. doi: 10.3791/2059 [PubMed: 20972389]

Matsumoto H, Sugio S, Seghers F, Krizaj D, Akiyama H, Ishizaki Y, … Shibasaki K (2018). Retinal detachment-induced Müller glial cell swelling activates TRPV4 ion channels and triggers photoreceptor death at body temperature. The Journal of Neuroscience, 38(41), 8745–8758. doi: 10.1523/jneurosci.0897-18.2018 [PubMed: 30143574]

Matthews BD, Thodeti CK, Tytell JD, Mammoto A, Overby DR, & Ingber DE (2010). Ultra-rapid activation of TRPV4 ion channels by mechanical forces applied to cell surface β1 integrins. Integrative Biology, 2(9), 435–442. Doi: 10.1039/c0ib00034e [PubMed: 20725677]

Mola MG, Sparaneo A, Gargano CD, Spray DC, Svelto M, Frigeri A, … Nicchia GP (2015). The speed of swelling kinetics modulates cell volume regulation and calcium signaling in astrocytes: A different point of view on the role of aquaporins. Glia, 64(1), 139–154. doi: 10.1002/glia.22921 [PubMed: 26413835]

Molnar T, Barabas P, Birnbaumer L, Punzo C, Kefalov V, & Križaj D (2012). Store-operated channels regulate intracellular calcium in mammalian rods. The Journal of Physiology, 590(15), 3465–3481. doi: 10.1113/jphysiol.2012.234641 [PubMed: 22674725]

Molnár T, Yarishkin O, Iuso A, Barabas P, Jones B, Marc RE, … Krizaj D (2016). Store-operated calcium entry in Müller glia is controlled by synergistic activation of TRPC and Orai channels. The Journal of Neuroscience, 36(11), 3184–3198. doi: 10.1523/jneurosci.4069-15.2016 [PubMed: 26985029]

Mongin AA (2015). Volume-regulated anion channel—a frenemy within the brain. Pflügers Archiv - European Journal of Physiology, 468(3), 421–441. doi: 10.1007/s00424-015-1765-6 [PubMed: 26620797]

Morihata H, Kawawaki J, Sakai H, Sawada M, Tsutada T, & Kuno M (2000). Temporal fluctuations of voltage-gated proton currents in rat spinal microglia via pH-dependent and -independent mechanisms. Neuroscience Research, 38(3), 265–271. doi: 10.1016/s0168-0102(00)00170-x [PubMed: 11070193]

Murphy TR, Davila D, Cuvelier N, Young LR, Lauderdale K, Binder DK, & Fiacco TA (2017). Hippocampal and cortical pyramidal neurons swell in parallel with astrocytes during acute hypoosmolar stress. Frontiers in Cellular Neuroscience, 11, 275. doi: 10.3389/fncel.2017.00275 [PubMed: 28979186]

Nakai J, Ohkura M, & Imoto K (2001). A high signal-to-noise Ca2+ probe composed of a single green fluorescent protein. Nature Biotechnology, 19(2), 137–141. doi: 10.1038/84397

Neher E (1995). The use of fura-2 for estimating Ca buffers and Ca fluxes. Neuropharmacology, 34, 972–981. doi:10.1016/0028-3908(95)00144-u

Nimmerjahn A, Kirchhoff F, & Helmchen F (2005). Resting microglial cells are highly dynamic surveillants of brain parenchyma in vivo. Science, 308(5726), 1314–1318. doi: 10.1126/science.1110647 [PubMed: 15831717]

O'Koren EG, Yu C, Klingeborn M, Wong AYW, Prigge CL, Mathew R, Kalnitsky J, Msallam RA, Silvin A, Kay JN, Bowes Rickman C, Arshavsky VY, Ginhoux F, Merad M, Saban DR (2019). Microglial Function Is Distinct in Different Anatomical Locations during Retinal Homeostasis and Degeneration. Immunity 50(3):723–737.e7 doi: 10.1016/j.immuni.2019.02.007 [PubMed: 30850344]

Orr AG, Orr AL, Li X, Gross RE, & Traynelis SF (2009). Adenosine A(2A) receptor mediates microglial process retraction. Nature Neuroscience, 12(7), 872–878. doi: 10.1038/nn.2341 [PubMed: 19525944]

Otani T, Yamaguchi Y, & Kishi S (2010). Correlation between visual acuity and foveal microstructural changes in diabetic macular edema. Retina, 30(5), 774–780. doi: 10.1097/IAE.0b013e3181c2e0d6 [PubMed: 19996821]

Pannicke T, Iandiev I, Wurm A, Uckermann O, Hagen FV, Reichenbach A, … Bringmann A (2006). Diabetes alters osmotic swelling characteristics and membrane conductance of glial cells in rat retina. Diabetes, 55(3), 633–639. doi: 10.2337/diabetes.55.03.06.db05-1349 [PubMed: 16505225]

Phuong TTT, Redmon SN, Yarishkin O, Winter JM, Li DY, & Križaj D (2017). Calcium influx through TRPV4 channels modulates the adherens contacts between retinal microvascular endothelial cells. The Journal of Physiology, 595(22), 6869–6885. doi: 10.1113/jp275052 [PubMed: 28949006]

Pozner A, Xu B, Palumbos S, Gee JM, Tvrdik P, & Capecchi MR (2015). Intracellular calcium dynamics in cortical microglia responding to focal laser injury in the PC::G5-tdT reporter mouse. Frontiers in Molecular Neuroscience, 8, 12. doi: 10.3389/fnmol.2015.00012 [PubMed: 26005403]

Ré DB, & Przedborski S (2006). Fractalkine: Moving from chemotaxis to neuroprotection. Nature Neuroscience, 9(7), 859–861. doi: 10.1038/nn0706-859 [PubMed: 16801915]

Redmon S, Shibasaki K, & Krizaj D (2017). Transient receptor potential cation channel subfamily V member 4 (TRPV4). In Choi S (Ed.), Encyclopedia of Signaling Molecules (2nd ed.). Springer Nature.

Renneboog B, Musch W, Vandemergel X, Manto MU, & Decaux G (2006). Mild chronic hyponatremia is associated with falls, unsteadiness, and attention deficits. The American Journal of Medicine, 119(1), 71.e1–71.e718. doi: 10.1016/j.amjmed.2005.09.026

Risher WC, Andrew RD, & Kirov SA (2009). Real-time passive volume responses of astrocytes to acute osmotic and ischemic stress in cortical slices and in vivo revealed by two-photon microscopy. Glia, 57(2), 207–221. doi: 10.1002/glia.20747 [PubMed: 18720409]

Ryskamp DA, Witkovsky P, Barabas P, Huang W, Koehler C, Akimov NP, … Krizaj D (2011). The polymodal ion channel transient receptor potential vanilloid 4 modulates calcium flux, spiking rate, and apoptosis of mouse retinal ganglion cells. The Journal of Neuroscience, 31(19), 7089–7101. doi: 10.1523/jneurosci.0359-11.2011 [PubMed: 21562271]

Ryskamp DA, Jo AO, Frye AM, Vazquez-Chona F, Macaulay N, Thoreson WB, & Križaj D (2014). Swelling and eicosanoid metabolites differentially gate TRPV4 channels in retinal neurons and glia. The Journal of Neuroscience, 34(47), 15689–15700. doi: 10.1523/jneurosci.2540-14.2014 [PubMed: 25411497]

Ryskamp DA, Frye AM, Phuong TTT, Yarishkin O, Jo AO, Xu Y, … Križaj D (2016). TRPV4 regulates calcium homeostasis, cytoskeletal remodeling, conventional outflow and intraocular pressure in the mammalian eye. Scientific Reports, 6, 30583. doi: 10.1038/srep30583 [PubMed: 27510430]

Salter MW, & Stevens B (2017). Microglia emerge as central players in brain disease. Nature Medicine, 23(9), 1018–1027. doi: 10.1038/nm.4397

Scheraga RG, Southern BD, Grove LM, & Olman MA (2017). The role of transient receptor potential vanilloid 4 in pulmonary inflammatory diseases. Frontiers in Immunology, 8, 503. doi: 10.3389/fimmu.2017.00503 [PubMed: 28523001]

Schindelin J, Arganda-Carreras I, Frise E, Kaynig V, Longair M, Pietzsch T, … Cardona A (2012). Fiji: An open-source platform for biological-image analysis. Nature Methods, 9(7), 676–682. doi: 10.1038/nmeth.2019 [PubMed: 22743772]

Schlichter LC, Mertens T, & Liu B (2011). Swelling activated Cl^- channels in microglia: Biophysics, pharmacology and role in glutamate release. Channels (Austin), 5(2), 128–137. doi: 10.4161/chan.5.2.14310 [PubMed: 21150294]

Schneidereit D, Vass H, Reischl B, Allen RJ, & Friedrich O (2016). Calcium sensitive fluorescent dyes fluo-4 and fura red under pressure: Behaviour of fluorescence and buffer properties under hydrostatic pressures up to 200 MPa. Plos One, 11(10), e0164509. doi: 10.1371/journal.pone.0164509 [PubMed: 27764134]

Shibasaki K (2020). TRPV4 activation by thermal and mechanical stimuli in disease progression. Lab Invest. 100(2):218–223 doi: 10.1038/s41374-019-0362-2. [PubMed: 31896814]

Shuttleworth TJ (2009). Arachidonic acid, ARC channels, and Orai proteins. Cell Calcium, 45(6), 602–610. doi: 10.1016/j.ceca.2009.02.001 [PubMed: 19278724]

Silvin A, Ginhoux F (2018). Microglia heterogeneity along a spatio-temporal axis: More questions than answers. Glia 66(10), 2045–2057. [PubMed: 30144321]

Sołtys Z, Ziaja M, Pawliński R, Setkowicz Z, & Janeczko K (2001). Morphology of reactive microglia in the injured cerebral cortex. Fractal analysis and complementary quantitative methods. Journal of Neuroscience Research, 63(1), 90–97. doi: 10.1002/1097-4547(20010101)63:1<90::aid-jnr11>3.0.co;2-9 [PubMed: 11169618]

Sonkusare SK, Bonev AD, Ledoux J, Liedtke W, Kotlikoff MI, Heppner TJ, … Nelson MT (2012). Elementary Ca2+ signals through endothelial TRPV4 channels regulate vascular function. Science, 336(6081), 597–601. doi: 10.1126/science.1216283 [PubMed: 22556255]

Srinivasan R, Huang BS, Venugopal S, Johnston AD, Chai H, Zeng H, … Khakh BS (2015). Ca2+ signaling in astrocytes from Ip3r2−/− mice in brain slices and during startle responses in vivo. Nature Neuroscience, 18(5), 708–717. doi: 10.1038/nn.4001 [PubMed: 25894291]

Starkey J, Kobayashi N, Numaguchi Y, & Moritani T (2017). Cytotoxic lesions of the corpus callosum that show restricted diffusion: Mechanisms, causes, and manifestations. RadioGraphics, 37(2), 562–576. doi: 10.1148/rg.2017160085 [PubMed: 28165876]

Staub F, Winkler A, Peters J, Kempski O, & Baethmann A (1994). Mechanisms of glial swelling by arachidonic acid. Acta neurochirurgica. Supplementum, 60, 20–23. doi: 10.1007/978-3-7091-9334-1_5 [PubMed: 7976545]

Strotmann R, Harteneck C, Nunnenmacher K, Schultz G, & Plant TD (2000). OTRPC4, a nonselective cation channel that confers sensitivity to extracellular osmolarity. Nature Cell Biology, 2(10), 695–702. doi: 10.1038/35036318 [PubMed: 11025659]

Sun JK, Radwan SH, Soliman AZ, Lammer J, Lin MM, Prager SG, … Aiello LP (2015). Neural retinal disorganization as a robust marker of visual acuity in current and resolved diabetic macular edema. Diabetes, 64(7), 2560–2570. doi: 10.2337/db14-0782. [PubMed: 25633419]

Szikra T, Barabas P, Bartoletti TM, Huang W, Akopian A, Thoreson WB, & Krizaj D (2009). Calcium homeostasis and cone signaling are regulated by interactions between calcium stores and plasma membrane ion channels. PLoS ONE, 4(8), e6723. doi: 10.1371/journal.pone.0006723 [PubMed: 19696927]

Tanaka M, Ishihara Y, Mizuno S, Ishida A, Vogel CF, Tsuji M, … Itoh K (2018). Progression of vasogenic edema induced by activated microglia under permanent middle cerebral artery occlusion. Biochemical and Biophysical Research Communications, 496(2), 582–587. doi: 10.1016/j.bbrc.2018.01.094 [PubMed: 29353043]

Tang XN, Zheng Z, Giffard RG, & Yenari MA (2011). Significance of marrow derived NADPH oxidase in experimental ischemic stroke. Annals of Neurology, 70(4), 606–615. doi: 10.1002/ana.22476 [PubMed: 22028221]

Taylor L, Arnér K, & Ghosh F (2017). Specific inhibition of TRPV4 enhances retinal ganglion cell survival in adult porcine retinal explants. Experimental Eye Research, 154, 10–21. doi: 10.1016/j.exer.2016.11.002 [PubMed: 27816538]

Thorneloe KS, Cheung M, Bao W, Alsaid H, Lenhard S, Jian M-Y, … Willette RN (2012). An orally active TRPV4 channel blocker prevents and resolves pulmonary edema induced by heart failure. Science Translational Medicine, 4(159), 159ra148. doi: 10.1126/scitranslmed.3004276

Tian W, Fu Y, Garcia-Elias A, Fernandez-Fernandez JM, Vicente R, Kramer PL, … Cohen DM (2009). A loss-of-function nonsynonymous polymorphism in the osmoregulatory TRPV4 gene is associated with human hyponatremia. Proceedings of the National Academy of Sciences, 106(33), 14034–14039. doi: 10.1073/pnas.0904084106

Toft-Bertelsen TL, Križaj D, & Macaulay N (2017). When size matters: transient receptor potential vanilloid 4 channel as a volume-sensor rather than an osmo-sensor. The Journal of Physiology, 595(11), 3287–3302. doi: 10.1113/jp274135 [PubMed: 28295351]

Toft-Bertelsen TL, Yarishkin O, Redmon S, Phuong TTT, Krizaj D, & MacAulay N (2019). Volume sensing in the transient receptor potential vanilloid 4 ion channel is cell type-specific and mediated by an N-terminal volume-sensing domain. Journal of Biological Chemistry, 294(48), 18421–18434. doi: 10.1074/jbc.RA119.011187

Tvrdik P, & Kalani M (2017). In vivo imaging of microglial calcium signaling in brain inflammation and injury. International Journal of Molecular Sciences, 18(11), 2366. doi: 10.3390/ijms18112366

Umpierre AD, Bystrom LL, Ying Y, Liu YU, Worrell G, & Wu L (2020). Microglial calcium signaling is attuned to neuronal activity in awake mice. eLife, 9, e56502. doi: 10.7554/eLife.56502 [PubMed: 32716294]

Wake H, Moorhouse AJ, Jinno S, Kohsaka S, & Nabekura J (2009). Resting microglia directly monitor the functional state of synapses in vivo and determine the fate of ischemic terminals. The Journal of Neuroscience, 29(13), 3974–3980. doi: 10.1523/jneurosci.4363-08.2009 [PubMed: 19339593]

Wang X, Zhao L, Zhang J, Fariss RN, Ma W, Kretschmer F, … Wong WT (2016). Requirement for microglia for the maintenance of synaptic function and integrity in the mature retina. The Journal of Neuroscience, 36(9), 2827–2842. doi: 10.1523/jneurosci.3575-15.2016 [PubMed: 26937019]

Watanabe H, Vriens J, Prenen J, Droogmans G, Voets T, & Nilius B (2003). Anandamide and arachidonic acid use epoxyeicosatrienoic acids to activate TRPV4 channels. Nature, 424(6947), 434–438. doi: 10.1038/nature01807 [PubMed: 12879072]

White JPM, Cibelli M, Urban L, Nilius B, Mcgeown JG, & Nagy I (2016). TRPV4: Molecular conductor of a diverse orchestra. Physiological Reviews, 96(3), 911–973. doi: 10.1152/physrev.00016.2015 [PubMed: 27252279]

Wittbrodt MT, Sawka MN, Mizelle JC, Wheaton LA, & Millard-Stafford ML (2018). Exercise-heat stress with and without water replacement alters brain structures and impairs visuomotor

performance. Physiological Reports, 6(16), e13805. doi: 10.14814/phy2.13805 [PubMed: 30136401]

Wolf SA, Boddeke H, & Kettenmann H (2017). Microglia in physiology and disease. Annual Review of Physiology, 79(1), 619–643. doi: 10.1146/annurev-physiol-022516-034406

Wright AR, & Rees SA (1997). Targeting ischaemia—cell swelling and drug efficacy. Trends in Pharmacological Sciences, 18(7), 224–228. Doi: 10.1016/s0165-6147(97)01078-x [PubMed: 9253851]

Wurm A, Pannicke T, Iandiev I, Francke M, Hollborn M, Wiedemann P, … Bringmann A (2011). Purinergic signaling involved in Müller cell function in the mammalian retina. Progress in Retinal Eye Research, 30(5):324–342. Doi: 10.1016/j.preteyeres.2011.06.001 [PubMed: 21689780]

Xiao D, Vanni MP, Mitelut CC, Chan AW, Ledue JM, Xie Y, … Murphy TH (2017). Mapping cortical mesoscopic networks of single spiking cortical or sub-cortical neurons. eLife, 6, e19976. doi: 10.7554/elife.19976 [PubMed: 28160463]

Yarishkin O, Phuong TTT, Lakk M, & Križaj D (2018). TRPV4 does not regulate the distal retinal light response. Advances in Experimental Medicine and Biology, 1074, 553–560. doi: 10.1007/978-3-319-75402-4_67 [PubMed: 29721987]

Yarishkin O, Phuong TTT, Baumann JM, De Ieso ML, Vazquez-Chona F, Rudzitis CN, … Krizaj D (2020). Piezo1 channels mediate trabecular meshwork mechanotransduction and promote aqueous fluid outflow. Journal of Physiology. Advance online publication. doi: 10.1113/JP281011

Ye L, Kleiner S, Wu J, Sah R, Gupta RK, Banks AS, … Spiegelman BM (2012). TRPV4 is a regulator of adipose oxidative metabolism, inflammation and energy homeostasis. Cell, 151(1), 96–110. Doi: 10.1016/j.cell.2012.08.034 [PubMed: 23021218]

Yu C, Roubeix C, Sennlaub F, & Saban DR (2020). Microglia versus monocytes: distinct roles in degenerative diseases of the retina. Trends in Neurosciences, 43(6), 433–449. doi: 10.1016/j.tins.2020.03.012 [PubMed: 32459994]

Zemtsova I, Görg B, Keitel V, Bidmon H-J, Schrör K, & Häussinger D (2011). Microglia activation in hepatic encephalopathy in rats and humans. Hepatology, 54(1), 204–215. doi: 10.1002/hep.24326 [PubMed: 21452284]

Zhang Y, Chen K, Sloan SA, Bennett ML, Scholze AR, Okeeffe S, … Wu JQ (2014). An RNA-sequencing transcriptome and splicing database of glia, neurons, and vascular cells of the cerebral cortex. The Journal of Neuroscience, 34(36), 11929–11947. doi: 10.1523/jneurosci.1860-14.2014 [PubMed: 25186741]

Zhao H, Zhang K, Tang R, Meng H, Zou Y, Wu P, … Chen Y (2018). TRPV4 blockade preserves the blood–brain-barrier by inhibiting stress fiber formation in a rat model of intracerebral hemorrhage. Frontiers in Molecular Neuroscience, 11, 97. doi: 10.3389/fnmol.2018.00097 [PubMed: 29636662]

Zierler S, Frei E, Grissmer S, & Kerschbaum HH (2008). Chloride influx provokes lamellipodium formation in microglial cells. Cellular Physiology and Biochemistry, 21(1–3), 55–62. doi: 10.1159/000113747 [PubMed: 18209472]

Main Points

- TRPV4 mediates response to physiological and pathological osmogradients and strains in retinal microglia.
- Its activation inhibits microglial ramification and is PLA2-dependent.
- Microglial TRPV4 may link CNS edema with inflammatory signaling.

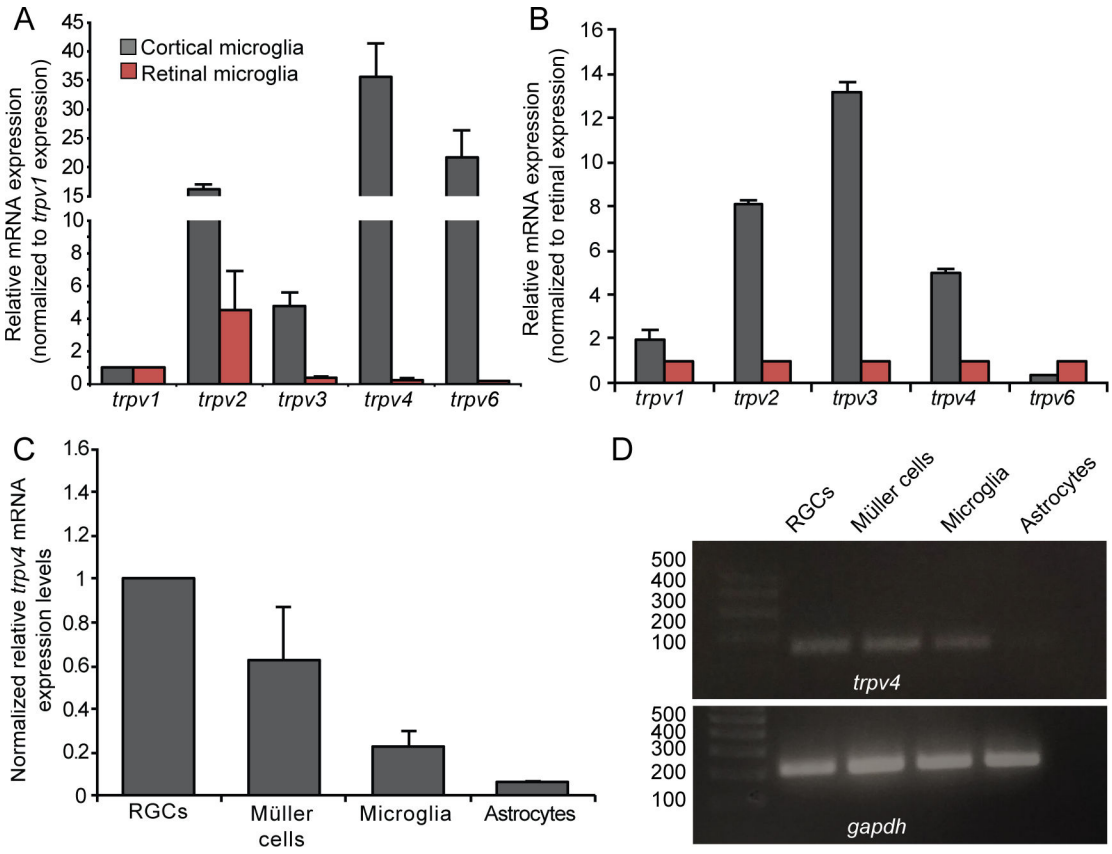

Figure 1. Retinal microglia express mRNAs coding for multiple vanilloid TRP isoforms.

(A) Semi-quantitative real-time PCR for cortical retinal microglial *trpv* transcripts normalized *to trpv1* expression. (B) Semi-quantitative real-time PCR for other retinal cell type *trpv4* expression levels were normalized to neuronal *trpv4* expression levels. (C) Representative agarose gel image of PCR products obtained in (B). Error bars represent mean ± S.E.M.

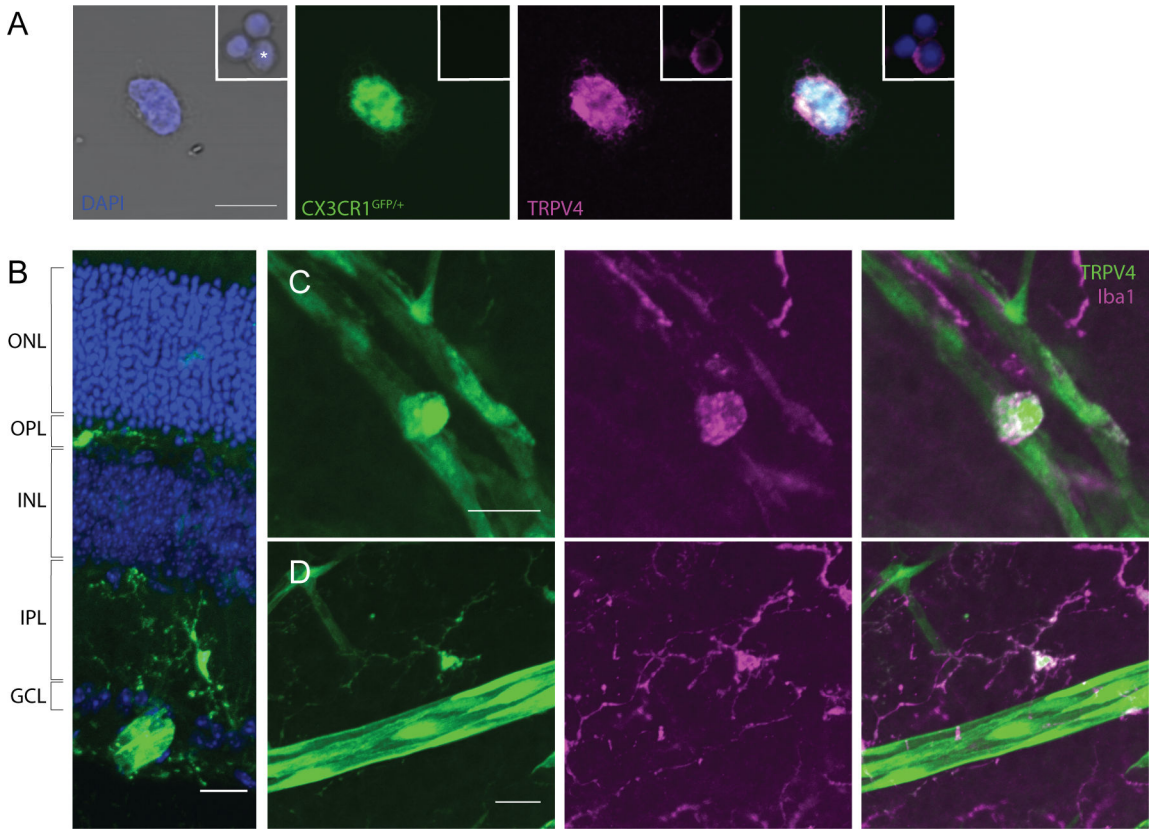

Figure 2. TRPV4 is expressed in retinal microglia.

(A) Representative images of TRPV4 IHC in dissociated microglia. Dissociated microglia could be distinguished from photoreceptors and RGCs (*) by morphology and expression of CX3CR1$^{GFP/+}$. (B) Vertical section of mouse retina expressing TRPV4^{eGFP}. Microglia are identifiable by morphology and localization to the retinal ganglion cell/nerve fiber and the inner and outer plexiform layers (C-D) Retinal wholemounts expressing TRPV4^{eGFP} and immunolabeled for Iba1 (magenta; C-D, middle panels) revealed robust expression in both reactive (C) and quiescent (D) microglia. Scale bar is 20 μm in B-D; 10 μm in A. onl, outer nuclear layer; opl, outer plexiform layer, inl, inner nuclear layer, ipl, inner plexiform layer, gcl, ganglion cell layer.

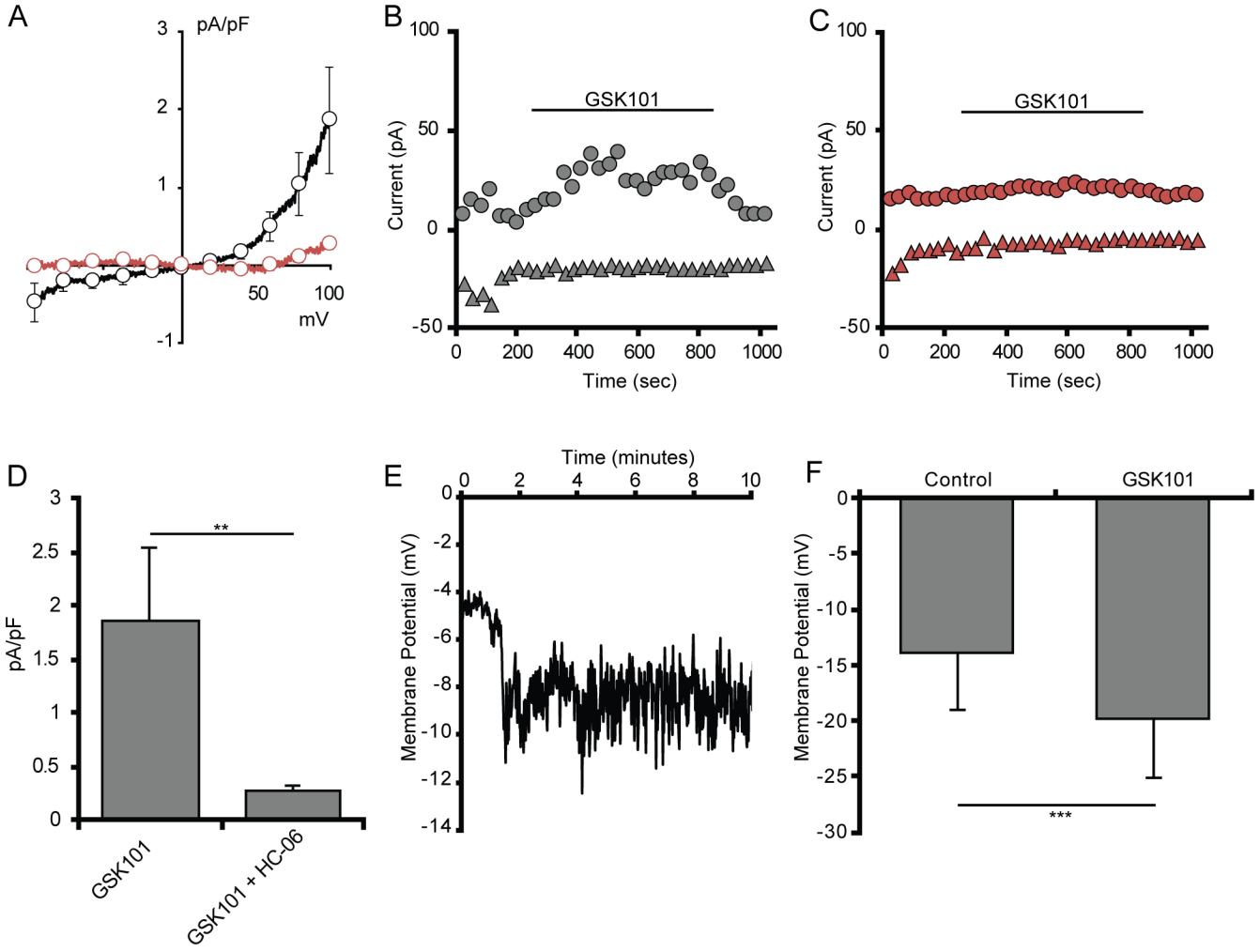

Figure 3. Selective TRPV4 agonists induce cation currents in retinal microglia.

(A) Average I-V curve of GSK101-induced currents in acutely dissociated microglia (n = 4). (B) Average I-V curve of GSK101-induced currents in *in situ* microglia either untreated (n = 6, black trace) or treated with HC-06 (n = 6, red trace). GSK101-induced currents were obtained by subtraction of the currents before GSK101 application from the currents at the maximum response to GSK101. (C) Representative time course of whole-cell currents in an untreated microglia (gray) or a microglia pretreated with HC-06 (red) at 100 mV (circles) and −100 mV (triangles). (D) Quantification of GSK101-induced currents in *in situ* microglial cells untreated and treated with HC-06 (baselines currents were subtracted), with current amplitude values at −100 mV. (E) Quantification of GSK101-induced currents in dissociated microglial cells. (F) Representative trace of dissociated microglial membrane potential hyperpolarizing in response to GSK101. (G) Quantification of the change in membrane potential of retinal microglia (n = 4) exposed to GSK101. All values are represented as mean ± S.E.M. Statistical significance was determined with a paired-sample t-test, **p < 0.01, *** p < 0.001.

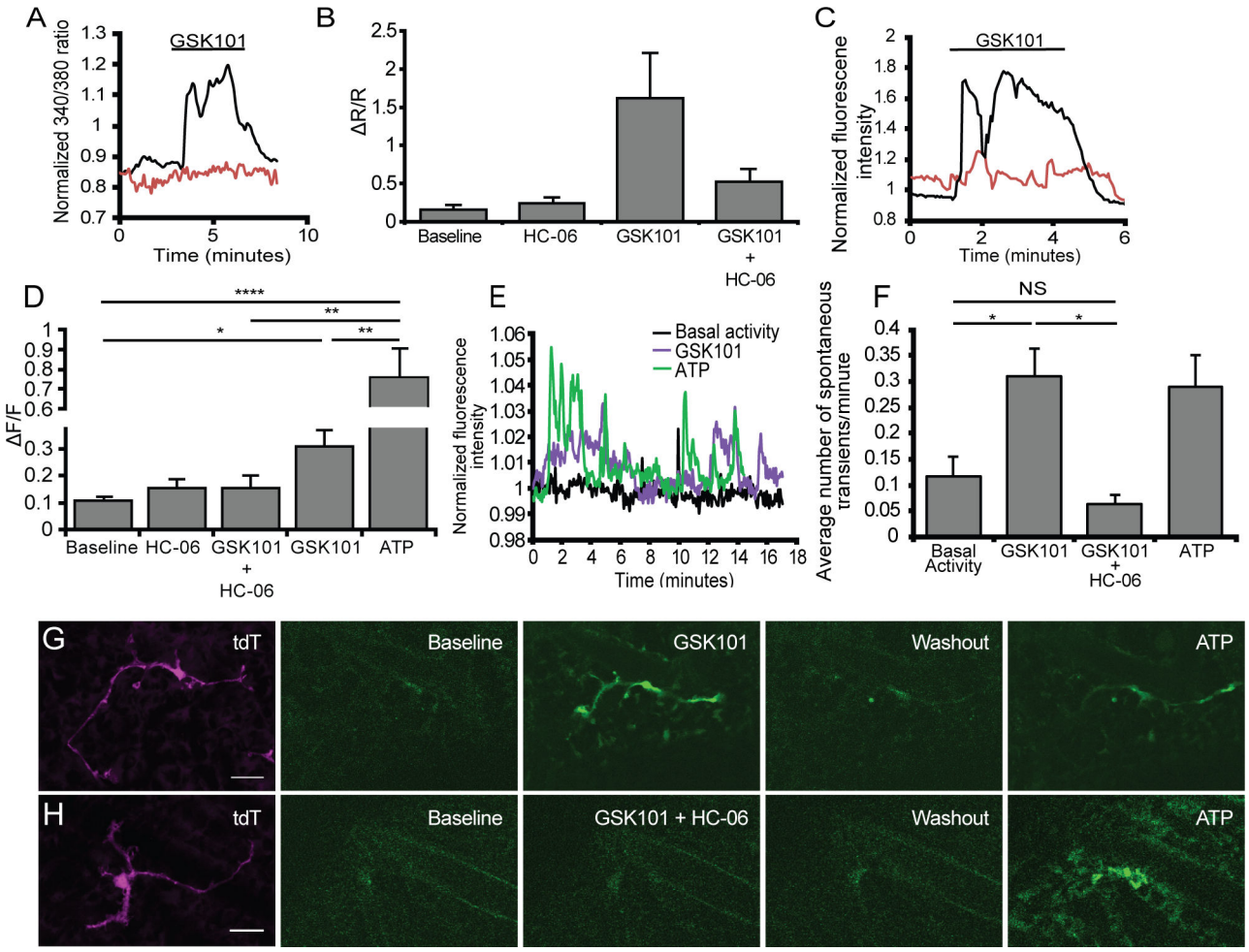

Figure 4. Microglia express functional TRPV4 channels.

(A) Representative trace from dissociated microglia loaded with Fura-2 exposed to GSK101 (black trace) of GSK101 in conjunction with HC-06 (red trace). (B) Quantification of changes in the 340/380 ratio in dissociated microglia treated with either GSK101 alone or GSK101 in the presence of HC-06 (n = 3–8). (C) Representative trace from *in situ* GCaMP5-expressing microglia exposed to GSK101 application (black trace) or GSK101 + HC-06 (red trace). (D) Quantification of changes in GCaMP5 fluorescence in the presence of GSK101 alone, with HC-06, HC-06 alone and ATP (n = 6–15). (E) Representative trace of spontaneous activity in a single microglial cell under resting conditions and when challenged with GSK101. (F) Quantification of the average number of spontaneous events in the presence of GSK101, GSK101 and HC-06 and ATP (n = 9–18). (G-H) Representative time lapse of changes in microglial GCaMP5 fluorescence in the presence GSK101 (G) or GSK101 + HC-06 (H). (H) All values are represented as mean ± S.E.M. Statistical significance was determined with a one-way ANOVA, and the post-hoc Holms-Šídák test for multiple comparisons (B, D) or a Kruskal Wallis test with Dunn's test for multiple comparisons (F). NS = non-significant, ** $p < 0.01$, *** $p < 0.001$, **** $p < 0.0001$. Scale bars in E-F are 20 μm.

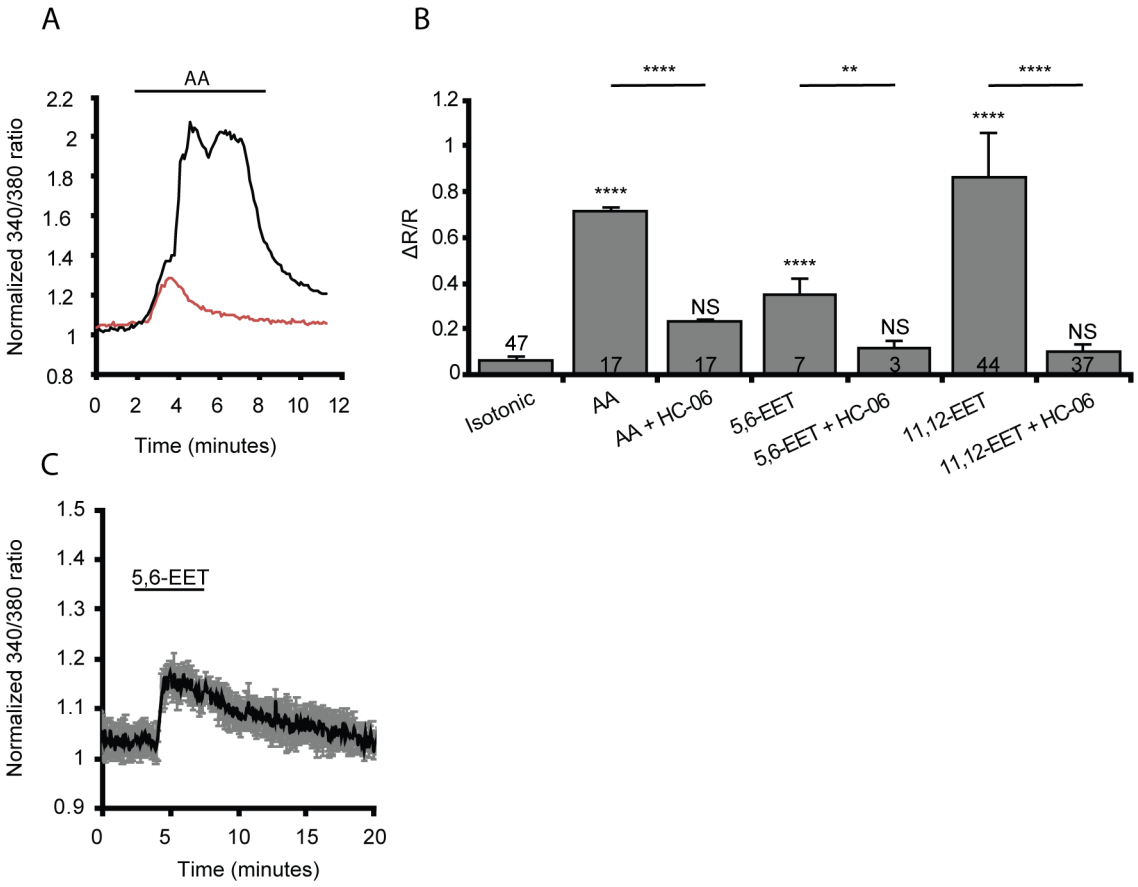

Figure 5. TRPV4 activation in microglia is dependent, in part, on the activation of arachidonic acid's metabolic cascade into epoxyeicosatrienoic acids (EETs).

(A) Representative trace of a dissociated microglial response to arachidonic acid (AA, black trace) or arachidonic acid + HC-06 (red trace). (B) Quantification of the change in 340/380 ratio in response to AA or its metabolites, 5,6-ET and 11,12-EET alone or administered with HC-06 (n = 3–47). Numbers inside bars represent the number of cells examined in each condition. (C) Average trace of dissociated microglia in response 5,6-EET. All values are represented by mean ± S.E.M. Statistical significance was determined with a Kruskal Wallis test with Dunn's test for multiple comparisons, NS = not significant, ** $p < 0.01$, **** $p < 0.0001$. Unless otherwise indicated statistical significance is compared to the isotonic condition.

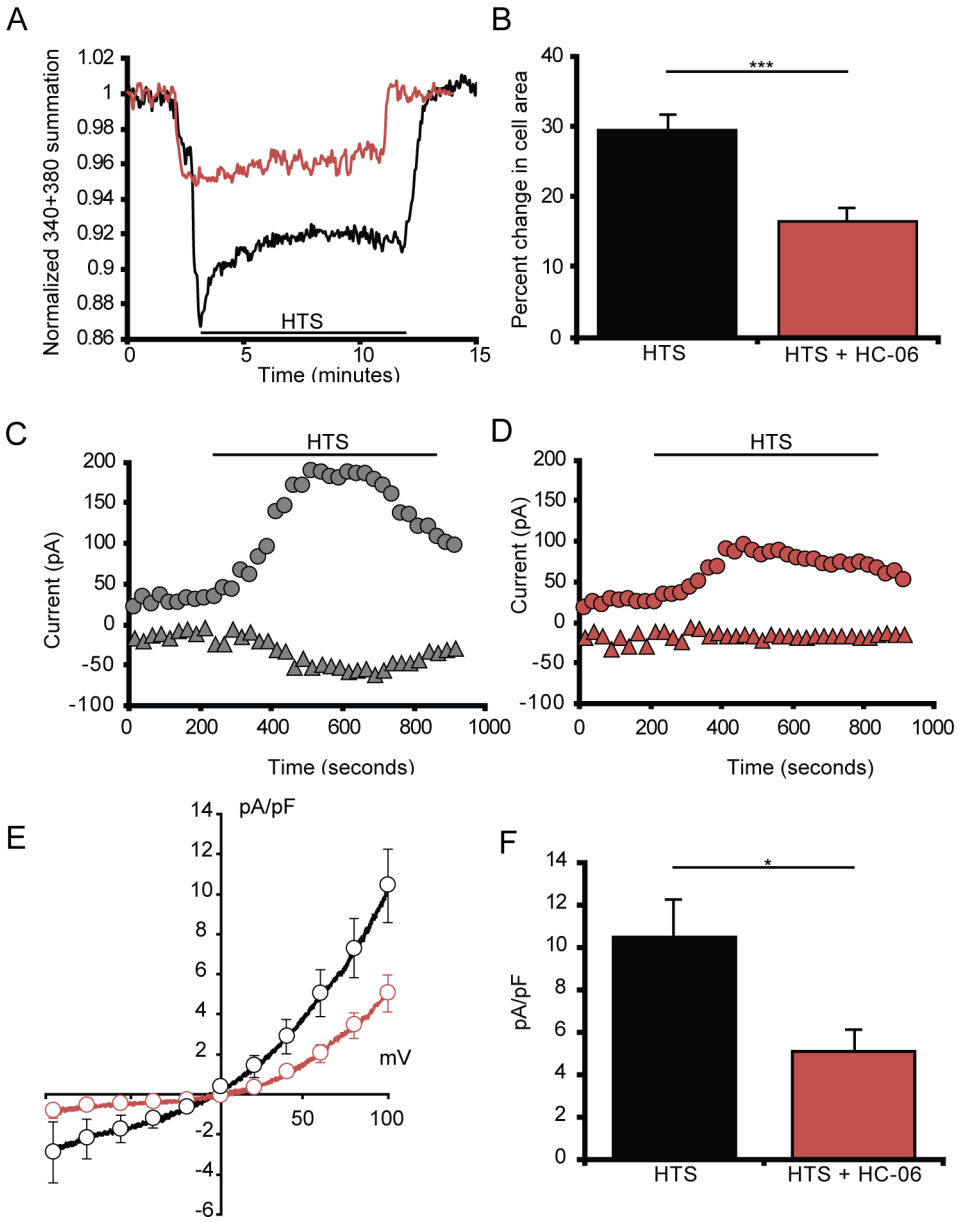

Figure 6. Dissociated microglia swell and exhibit cation currents when exposed to HTS.

(A) Dissociated microglia swell in response to HTS before undergoing regulatory volume decrease. (B) Quantification of the change in microglia volume when exposed to either HTS alone (n = 13) or HTS in the presence of HC-06 (n = 9) from isotonic conditions. (C-D) Representative time course of whole-cell currents in microglia exposed to HTS either alone (C) or pretreated with HC-06 (D) at 100 mV (circles) and −100 mV (triangles) (n = 12). (E) Averaged I-V curve of HTS-induced currents in microglial cells either untreated (black trace) or treated with HC-06 (red trace). HTS-induced currents were obtained by subtraction of the currents before HTS application from the currents at the maximum response to HTS. (F) Quantification of HTS-induced currents in microglial cells exposed to HTS with and without HC-06 (baseline currents were subtracted). Shown are the current amplitude

values at 100 mV. All values are represented as Mean ± S.E.M. Statistical significance was determined with an unpaired t-test (B) or paired t-test (F), * $p < 0.05$, *** $p < 0.001$.

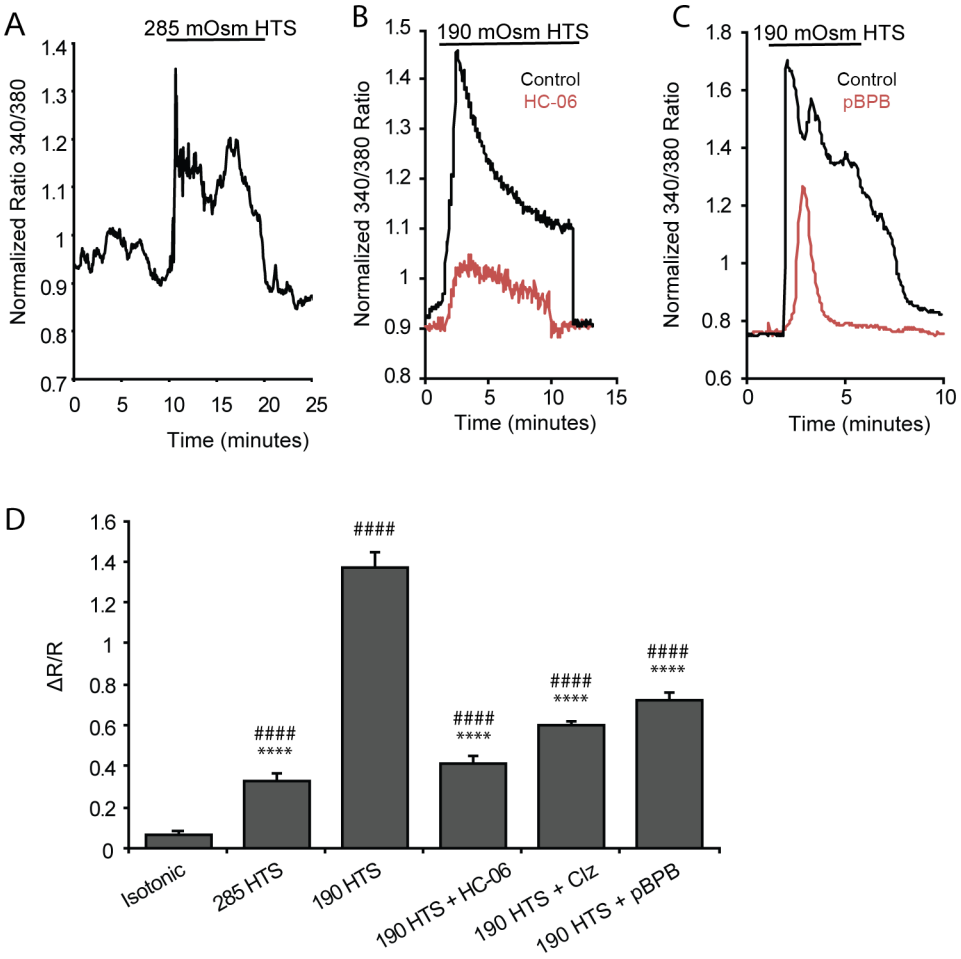

Figure 7. Calcium response induced by HTS stimulation requires TRPV4 activation and PLA2 signaling.

Dissociated microglia loaded with Fura-2 AM. (A) Representative trace of the microglial response to 285 mOsm HTS. (B) Representative microglial response to 190 mOsm HTS alone (black trace), and 190 mOsm HTS + HC-06 (red trace). (C) Microglial response to 190 mOsm HTS (black trace) and the presence of the PLA2 blocker p-bromophenacylbromide (pBPB) (red trace). (D) Summary of calcium responses to 285 and 190 mOsm HTS. The TRPV4-dependence of the HTS response was tested with HC-06, and PLA2-dependence with cytochrome P450 inhibitor clotrimazole (Clz) and pBPB. Data are shown as Mean ± S.E.M. Statistical significance was determined with a one-way ANOVA with Dunnett's test for multiple comparisons. * Statistical comparison to isotonic, # statistical comparison to HTS. **/## $p < 0.01$, ****/#### $p < 0.0001$

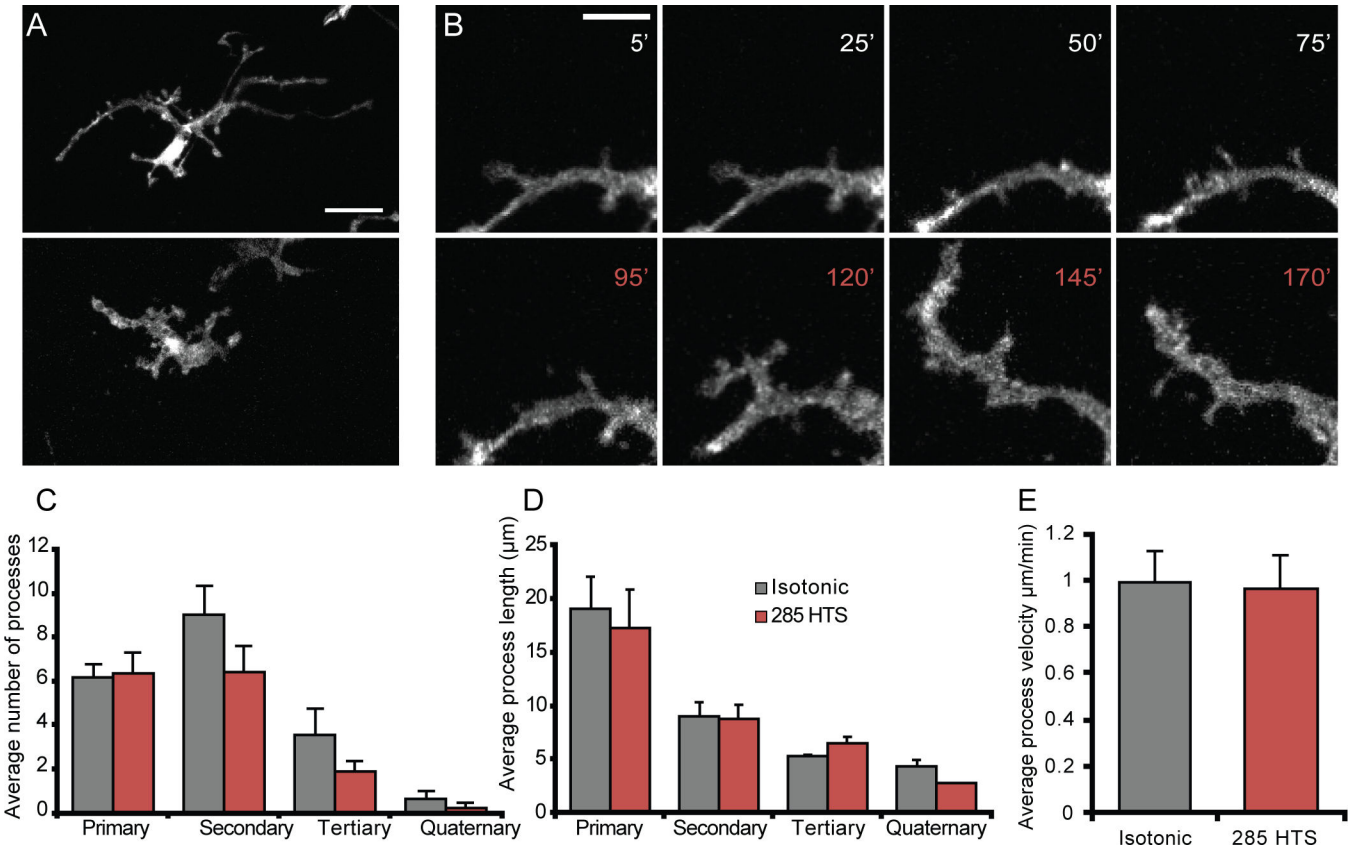

Figure 8. Decreasing the osmolarity by 5% induces subtle morphological changes in retinal microglia.

(A) Representative morphology of a retinal microglia imaged *ex vivo* when bathed in isotonic (top) or hypotonic (bottom). (B) Representative time-lapse 2P recording of a retinal microglial process during isotonic (white) or hypotonic (red) stimulation. (C-D) Quantification of the average number of processes per microglia (C) and average process length (D) during isotonic (n = 7), 285 mOsm hypotonic stimulation (n = 7), or 285 mOsm + HC-06 (n=5). Scale bar is 20 µm in A and 5 µm in B. All values are represented as mean ± S.E.M. Statistical significance for C and D was determined with a two-way ANOVA with Holms-Šídák's test for multiple comparisons. NS = non-significant, * $p < 0.05$, ** $p < 0.01$, **** $p < 0.0001$.

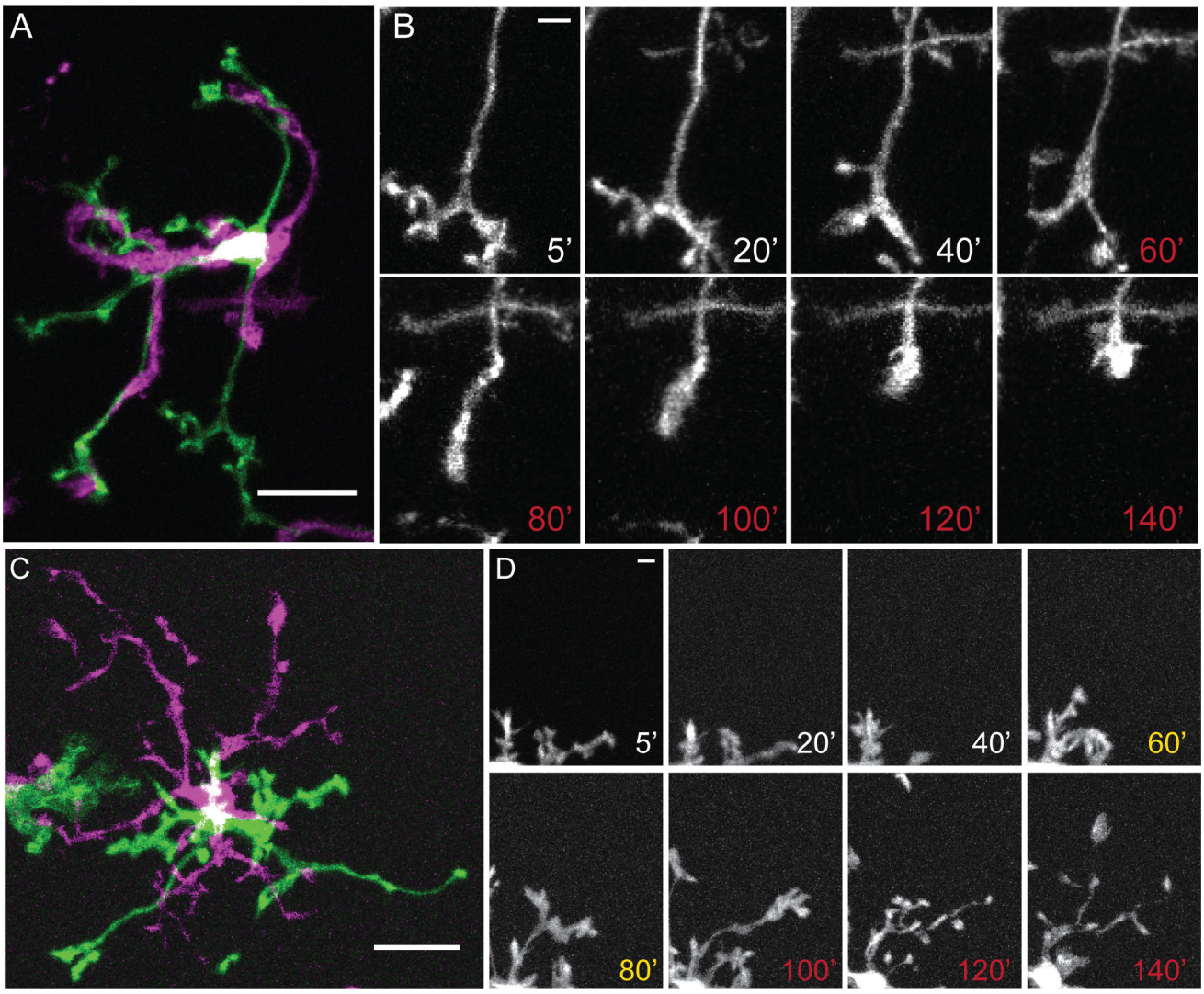

Figure 9. Decreasing the osmolarity by 36.7% results in retraction of complex branches and is rescued by selective TRPV4 antagonists.

(A) Representative microglia during isotonic (green) and hypotonic (magenta) stimuli. (B) Representative time lapse images of changing microglial processes during isotonic saline (white) or HTS (red). (C). Representative microglia during isotonic (green) or HTS after pretreatment with HC-06 (magenta). (D) Representative time lapse images of changing microglial processes during isotonic (white), pre-incubation with HC-06 (yellow) and HTS + HC-06 (red). Scale bar in A and C = 20 μm, B and D = 5 μm.

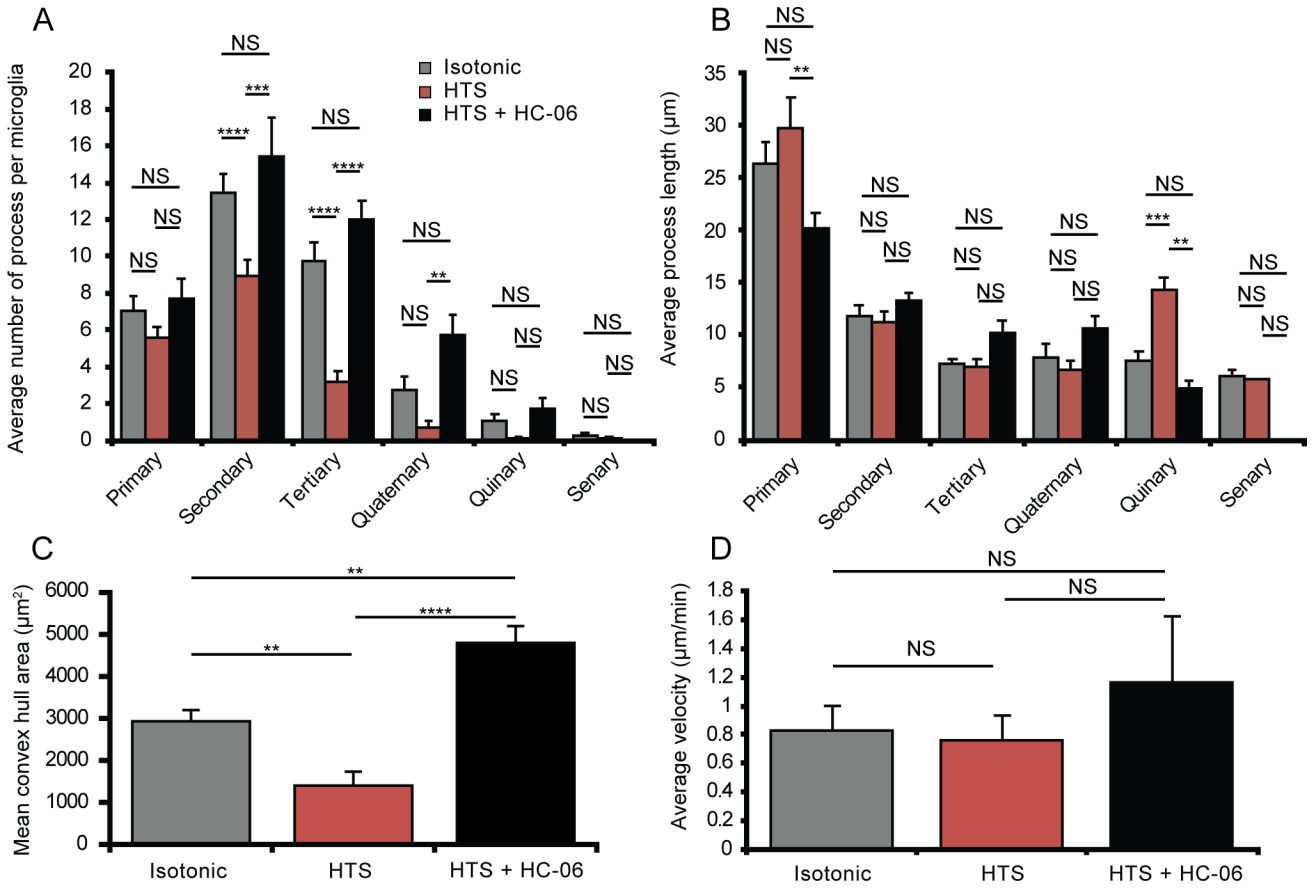

Figure 10. Decreasing the osmolarity by 36.7% results in retraction of complex branches and is rescued by selective TRPV4 antagonists.

(A-B) Quantification of microglial process complexity including the number of processes (A) and the average process length (B) when treated with isotonic (n = 19), HTS (n = 19) or HTS pretreated with HC-06 (n=4). (C) Quantification of the total area surveilled by microglial processes as represented by the mean convex hull. (D) Average velocity of microglial processes during each osmotic challenge with or without HC-06 (n = 9–13). All values are represented as Mean ± S.E.M. Statistical significance was determined with a two-way (A-B) or one-way (C) ANOVA with Holms-Šídak test for multiple comparisons. Statistical significance for (D) was determined with a Kruskal Wallis test with Dunn's test for multiple comparisons. NS = non-significant, * $p < 0.05$, ** $p < 0.01$, **** $p < 0.0001$.

Table 1.

Primer sequences used for semi-quantitative PCR in mouse microglia.

Name	Forward primer (5' → 3')	Reverse Primer (5' → 3')	NCBI Reference
mTRPV1	AGGGTGGATGAGGTGAACTGGACT	GCTGGGTGCTATGCCTATCTCG	NM_001001445.2
mTRPV2	GTTGGCCTACGTCCTCCTCACCTA	TGCACCACCAGTAACCATTCTCC	NM_011706.2
mTRPV3	CTCACCTTCGTCCTCCTCCTCAAC	CAGCCGGAAGTCCTCATCTGCTA	NM_145099.2
mTRPV4	TCCTGAGGCCGAGAAGTACA	TCCCCCTCAAACAGATTGGC	NM_022017.3
mTRPV6	GACTCTGTGGTCCGTGCCTCAT	CAGTGTTCTCCATCCGTCGTCTG	NM_022413.4
mActb	CCACCATGTACCCAGGCATT	AGGGTGTAAAACGCAGCTCA	NM_07393.4
mGapdh	GGTTGTCTCCTGCGACTTCA	TAGGGCCTCTCTTGCTCAGT	NM_001289726.1